Simulating snow properties and Ku-band backscatter across the forest-tundra ecotone.

Georgina J. Woolley[1], Nick Rutter[1], Leanne Wake[1], Vincent Vionnet[2], Chris Derksen[3], Julien Meloche[3], Benoit Montpetit[3], Nicolas R. Leroux[2], Richard Essery[4], Gabriel Hould Gosselin[1], Philip Marsh[5].

5   [1]Department of Geography and Environmental Sciences, Northumbria University, Newcastle Upon Tyne, UK.
[2]Meterological Research Division, Environment and Climate Change Canada, Dorval, QC, Canada.
[3]Climate Research Division, Environment and Climate Change Canada, Toronto, Canada.
[4]School of Geosciences, University of Edinburgh, Edinburgh, UK.
[5]Cold Regions Research Centre, Wilfrid Laurier University, Waterloo, Canada.

10   *Correspondence to*: Georgina J. Woolley (Georgina.j.woolley@northumbria.ac.uk).

Abstract.

Sophisticated snowpack models are required to provide accurate estimation of snowpack properties across the forest-tundra ecotone where in situ measurements are sparse. As snowpack properties strongly influence radar scattering signals, accurate simulation is crucial for the success of spaceborne radar missions to retrieve snow water equivalent (SWE). In this study, we

15   evaluate the ability of default and Arctic versions of Crocus embedded within the Soil, Vegetation and Snow version 2 (SVS2-Crocus) land surface model to simulate snowpack properties (e.g. depth, density, SWE, specific surface area; SSA) across a 40-km transect of the Northwest Territories, Canada, using two winter seasons (2021-22 & 2022-23) of in situ measurements. An ensemble of simulated snowpack properties (120 members from default and Arctic SVS2-Crocus) was used in the Snow Microwave Radiative Transfer (SMRT) model to simulate Ku-band (13.5 GHz) backscatter. Modelled backscatter using multi-

20   layer SVS2-Crocus snowpack simulations were compared to backscatter using a simplified 3-layer radar-equivalent snowpack. Results highlight that Arctic SVS2-Crocus wind-induced compaction modifications were spatially transferable across the forest-tundra ecotone, reducing the RMSE of surface density by an average of 29%. Basal vegetation modifications were less effective in simulating low-density basal snow layers at all sites (2022 & 2023; default RMSE: 67 kg m^{-3}; Arctic RMSE: 69 kg m^{-3}) but were necessary to simulate a physically representative Arctic density profile. SVS2-Crocus underestimated SSA

25   leading to high errors in the simulation of snow backscatter (2022 & 2023; default RMSE 3.5 dB; Arctic RMSE: 4.8 dB). RMSE of backscatter was reduced by implementing a minimum SSA value (8.7 m^2 kg^{-1}; 2022 & 2023; default RMSE: 1.5 dB; Arctic RMSE: 1.5 dB). A radar-equivalent snowpack was effective in retaining the scattering behaviour of the multi-layer snowpack (RMSE < 1 dB) providing a means to estimate SWE with increased computational efficiency.

1.0 Introduction

The forest-tundra ecotone represents a transition zone between areas of boreal forest and Arctic tundra (Callaghan et al., 2002). Rising air temperatures and altered precipitation patterns due to climate warming have led to rapid changes in vegetation composition and distribution across the forest-tundra ecotone (Graveline et al., 2024; Montesano et al., 2020), resulting in highly heterogeneous snow cover (Lackner et al., 2022). The structure and evolution of snowpack properties across the ecotone are poorly monitored because measurements of snow properties are sparse. Considering the rapid changes that are occurring across the forest-tundra ecotone, there is increasing need to explicitly simulate processes controlling evolution of snowpack properties through the use of snowpack models.

Differences in vegetation, topography and meteorological conditions across the forest-tundra ecotone generate spatially diverse snowpacks that display differences in microstructural properties (Lackner et al., 2022). Tundra snowpacks are exposed to high wind speeds and cold air temperatures leading to shallow snow depths (~40 cm; Derksen et al., 2014) with two dominant layers (Rutter et al., 2019; Derksen et al., 2009). High wind speeds compact the surface layers of the snowpack leading to the formation of high-density wind slab snow layers (King et al., 2020). Strong temperature gradients generate rapid metamorphism, redistributing mass through vapor transport and forming basal depth hoar layers (Bouvet et al., 2023; Weise, 2017). Shrub density increases southward across the forest-tundra ecotone (Ernakovich et al., 2014) resulting in deeper snow depths through the trapping effect of vegetation (Callaghan et al., 2012; Domine et al., 2016) and a reduction in snow density by inhibiting compaction (Royer et al., 2021b; Gouttevin et al., 2018; Barrere et al., 2017). Shrub branches that protrude through the surface of the snowpack can act as conducting thermal bridges, cooling the ground in winter (Domine et al., 2022) and impact the albedo of the snowpack surface (Ménard et al., 2014). In the boreal forest, canopy density influences the spatial variability of snowpack properties (Lackner et al., 2022). Beneath dense canopy, the snowpack is typically shallower due to interception of solid precipitation (Bouchard et al., 2022; Royer et al., 2021a). A shallower snowpack increases the temperature gradient, favouring depth hoar formation through water vapour transport (Bouchard et al., 2024). Under sparse forest canopy, the influence of snow interception and sublimation is low, combined with reduced wind speeds, deeper snow depths with low-density surface layers are found (Royer et al., 2021a; Lackner et al., 2022).

Accounting for all competing processes that contribute to the spatial diversity in snowpack properties observed across the forest-tundra ecotone within a snowpack model is possible, but the ability of such models to adequately simulate snowpack properties requires evaluation. The ability to simulate realistic vertical profiles of Arctic snowpack properties in tundra environments has been enhanced through the parameterisation of missing Arctic processes; wind-induced compaction and the presence of basal vegetation impacting compaction and metamorphism (Royer et al., 2021b; Domine et al., 2019; Barrere et al., 2017; Gouttevin et al., 2018; Lackner et al., 2022; Woolley et al., 2024). Optimal combinations of Arctic parameterisations that improve the simulation of snowpack properties at an Arctic site have been identified (Woolley et al., 2024) but are yet to

be tested in areas that differ in terms of vegetation, topography and meteorological conditions. The variability in snowpack properties across the forest-tundra ecotone has been measured in field campaigns (e.g. Royer et al., 2021a; Lackner et al.,

65 2022; Bouchard et al., 2022), but few model the impact of vegetation on simulated snowpack microstructure properties (Lackner et al., 2022). Under forest canopy, good agreement for the simulation of bulk density and SWE has been found (Bartlett et al., 2006; Oreiller et al., 2014), whereas uncertainties in the simulation of snow density still remain (Lackner et al., 2022; Bonner et al., 2022). Furthermore, the effect of shrubs (Barrere et al., 2017; Gouttevin et al., 2018; Royer et al., 2021b; Woolley et al., 2024) and canopy structure (Mazzotti et al., 2024; Sun et al., 2018) on snowpack properties has been included

70 within many snowpack schemes (Essery et al., 2024), allowing for important forest-snow interactions to be modelled.

Remote sensing can contribute to improved monitoring of snow across the forest-tundra ecotone, but current snow mass products are too coarse to spatially resolve the influence of landscape heterogeneity on snow distribution (Mortimer et al., 2020). Spaceborne radar missions could potentially contribute new snow information, but they require accurate information

75 on snowpack properties (e.g. specific surface area (SSA), density, layering) to retrieve SWE (Derksen et al., 2021; Tsang et al., 2022). Due to a lack of observation stations and ground-based measurements of snow microstructure (Sokol et al., 2003), simulation of snowpack properties across areas that differ in terms of vegetation, climatology and topography are therefore crucial to constrain the accuracy of SWE retrievals. Ku-band radar has been found to be sensitive to the snowpack microstructure, where a radiative transfer model (RTM) can be used to link snowpack properties to backscatter (Pan et al.,

80 2017; Cui et al., 2016). Significant progress has been made relating measurements of snowpack properties to backscatter (King et al., 2018; Lemmetyinen et al., 2018; Montpetit et al., 2024) but little work has focused on the impact of simulated snowpack information. A key variable in the retrieval of SWE is the number of snow model layers (Rutter et al., 2016), where large numbers of layers yields detailed information but at an increased computational cost. Recent studies show that similar scattering behaviour can be provided to the SWE retrieval using a simplified 3-layer snowpack through algorithms that retain

85 the bulk SWE and microwave scattering behaviour of the snowpack (Meloche et al., 2024; Pan et al., 2017). Linking a simplified simulated snowpack with backscatter through a RTM can therefore reduce the computational cost of SWE retrieval. This enables continuous SWE monitoring over continental scales, which is essential for environmental prediction, climate monitoring and water resource management (Garnaud et al., 2019; Kim et al., 2021).

90 This study evaluates the impact of changing vegetation across the forest-tundra ecotone on simulated snowpack properties (e.g. SWE, depth, density, profiles of density and SSA). Snow properties are simulated using the multi-physics ensemble version of Crocus (Lafaysse et al., 2017; Vionnet et al., 2012) embedded within the Soil, Vegetation and Snow version 2 land surface model (hereafter referred to as SVS2-Crocus; Vionnet et al., 2022; Woolley et al., 2024), driven by meteorological forcing data from the High Resolution Deterministic Prediction System (HRDPS; Milbrandt et al., 2016). SVS2-Crocus

95 simulations are compared to measurements at 7 sites across a 40-km transect of the Northwest Territories (NWT), Canada, that represent the transition from small shrubs to sparse evergreen needleleaf forest. The impact of an ensemble of simulated

snow microstructure properties on Ku-band (13.5 GHz) snow backscatter using the Snow Microwave Radiative Transfer Model (SMRT; Picard et al., 2018) is then tested for a multi-layer (~20 layers) and simplified (3-layer) microwave-equivalent snowpack derived using the technique of Meloche et al. (2024).

100 **2.0 Study Location**

A total of 7 sites spanning a 40-km transect across the NWT were selected to represent the variability in vegetation and snow conditions across the forest-tundra ecotone (Fig. 1 & 2). Among the 7 sites, 2 situated at the most northern edge of the transect were characterised as tundra (Fig. 1 & 2; Upper Plateau and Trail Valley Creek) with vegetation primarily consisting of low shrubs (0.1 – 0.7 m), lichens, grasses and mosses (King et al., 2018; Walker and Marsh, 2021; Marsh et al., 2010). Three sites

105 with scattered patches of grasses, mosses, birch and willow shrubs of varying heights (0.1 - 2 m) were distributed between tundra and forest sites to characterise the transition in vegetation across the ecotone and were classified as deciduous shrub (Fig. 1 & 2; Valley, Small Shrub, Mixed Shrub). Two further sites, characterised as forest, were selected at the most southern point of the transect covered by sparse evergreen needleleaf forest (canopy densities between 10 – 13 %) and open areas of tundra (Fig.1 & 2; Shrub Tree & Havikpak; Krogh and Pomeroy, 2019). The mean annual daily air temperature obtained from

110 the HRDPS was -16.8 ℃ over the 2021/22 winter and -16.9 ℃ over the 2022/23 winter, varying by 0.9 ℃ (2021/22) and 1.1 ℃ (2022/23) between sites. Maximum daily wind speed at 10 m above the surface was 4.8 m s^{-1} and 4.5 m s^{-1}, varying by 0.9 m s^{-1} and 0.7 m s^{-1} in the 2021/22 and 2022/23 winters, respectively. A significant snowfall event occurred late September in 2021, followed by gradual accumulation over the course of the winter (Fig. 3). The 2022/23 winter experienced consistent and gradual snowfall over the entire winter. Snowfall was higher in 2021/22 than in 2022/23, with the maximum cumulative

115 snowfall reaching 138 mm in 2021/22 and 113 mm 2022/23 at Shrub Tree (Fig. 3). Maximum snow accumulation between all sites varied by 21 mm in 2021/22 and 14 mm in 2023/23, with the lowest snowfall at TVC (Fig. 3).
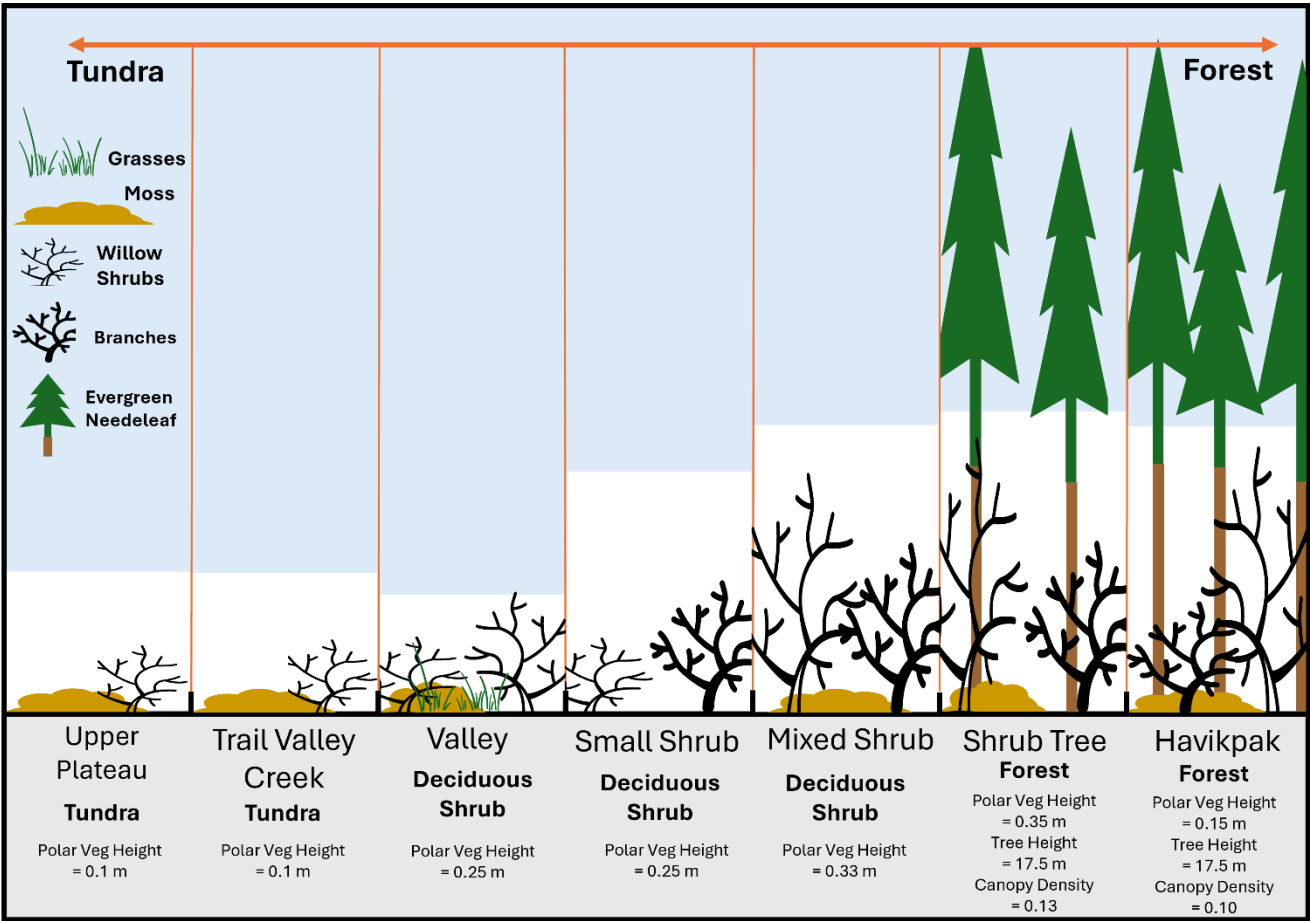
Figure 1: Schematic showing the variation in vegetation and relative snow depth (white bars) across a 40-km transect of the Northwest Territories, Canada (Fig. 2). SVS2-Crocus model parameters of vegetation type, polar vegetation height (see section 3.2.1 for definition), tree height and canopy density are also displayed for each site.
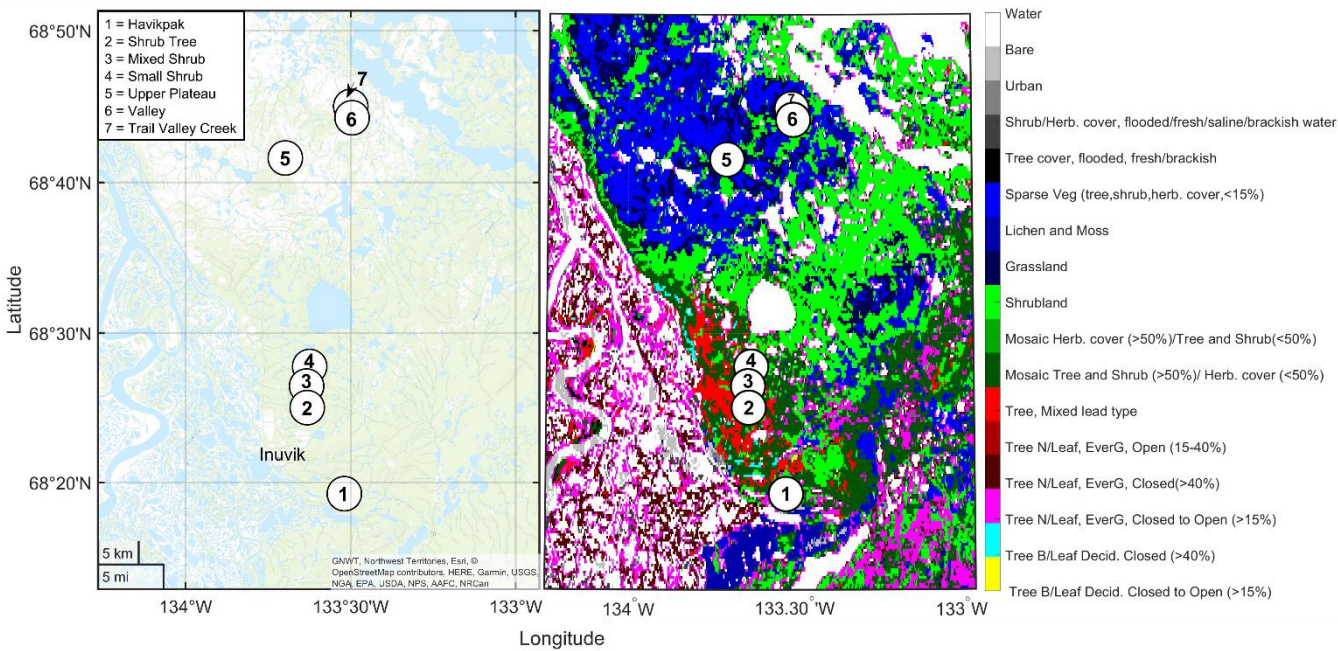
Figure 2: Map of the study domain showing (left) the location of the 7 sites across the 40-km transect of the Northwest Territories, Canada and (right) vegetation type at each site derived from the ESA CC1 LC global map (European Space Agency Climate Change Initiative Land Cover; http://esa-landcover-cci.org, last access: March 2025).
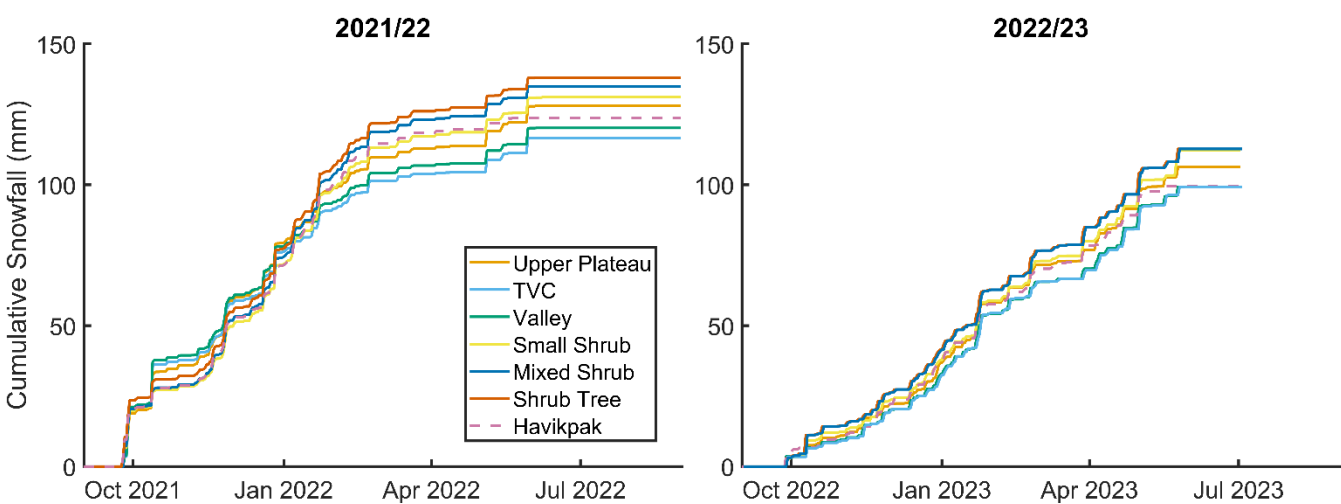
Figure 3: Cumulative snowfall (mm) obtained from the High-Resolution Deterministic Prediction System (HRDPS) for each site for the 2021/22 and 2022/23 winters.

3.0 Data and Methods

3.1 Field Methods

Over the 2021/22 and 2022/23 winters, snowpack properties were measured in snow pits (n = 66) around the time of peak SWE (late March). Snow pits were measured at the start, middle and end of a 1 km transect at each site, designed to capture

135 the spatial variability in snow properties. At all sites except Havikpak, one profile was conducted in each of the three snow pits during the 2021/22 season. Two profiles were conducted in each of the three snow pits during the 2022/23 season. At Havikpak, a 1 km transect was not possible due to forest cover. Instead, four profile locations were selected to represent the snow properties under forest canopy and in forest gaps. One profile was conducted in each of the four snow pits during the 2021/22 season, and two profiles were conducted in each of the four snow pits during the 2022/23 season at Havikpak. Profiles

140 of density using a 100 cm^3 density cutter and SSA using an A2 Photonic Sensor IceCube (Zuanon, 2013; Gallet et al., 2009) were measured at 3 cm vertical resolution. Snow temperature was measured using a stem thermometer at 10 cm intervals and snow stratigraphy identified by visual inspection following Fierz et al. (2009). At each of the 7 sites, snow depth distribution was measured along the 1 km transect (or between snow pits at Havikpak) using a Magnaprobe (~530 measurements per site; Sturm and Holmgren, 2018). Spirals around each pit were carried out at all non-forested sites (~270 measurements per site).

145 SWE measurements were made at 50 m intervals along each transect using a clear Lexan ESC-30 snow corer (Kinar and Pomeroy, 2015). The snow samples were weighted and depths recorded to provide the SWE at each sample point.

3.2 Modelling

3.2.1 SVS2-Crocus

The multi-physics ensemble version of the snowpack model Crocus (Brun et al., 1992; Lafaysse et al., 2017; Vionnet et al.,

150 2012) embedded within the Soil, Vegetation and Snow version 2 (SVS2) land surface model (Vionnet et al., 2022; Woolley et al., 2024) driven by meteorological forcing from the HRDPS was used to simulate the vertical layering and seasonal evolution of snowpack physical properties i.e. density, depth, SWE and SSA. Crocus computes the mass, density, temperature, liquid water content, age and snow microstructure properties (optical diameter, sphericity) of a multi-layer snowpack. Simulations were run from September 2020 to July 2023, with model spin-up of 5 years from September 2015 to allow soil temperatures

155 to equilibrate. Soil properties (sand/clay fraction) from the HRDPS geophysical fields were used to characterise the soil. Land cover type was specified based upon the metrics (vegetation type, polar vegetation height, tree height) presented in Fig. 1 & 2. The height of polar low vegetation, classified as the height of basal vegetation within each snowpit, was measured at each site ranging from 0.1 m to 0.35 m (Fig. 1). Canopy cover density values ranged from 10 to 13 % (Fig. 1), derived from hemispherical photographs taken at forested sites (Essery et al., 2008). The darkening coefficient in the snow albedo

160 parameterisation was modified from 60 d to 900 d within all simulations to account for a lower magnitude of light-absorbing impurities, associated fluxes and radiative forcing with Arctic snowpacks (Gaillard et al., 2025). Meteorological forcing data consisted of air temperature, specific humidity, wind speed, incoming longwave and shortwave radiation and solid and liquid

precipitation rates, which were obtained for each site from the HRDPS at 2.5 km grid spacing. Successive short-term HRDPS forecasts (7-12 hr lead time) were combined together to generate continuous hourly meteorological forcing.

165

The Ensemble System Crocus (ESCROC; Lafaysse et al., 2017) modelling framework within SVS2-Crocus allows model uncertainty due to parameterisation of snow processes within midlatitude environments to be investigated. However, the ESCROC ensemble does not consider Arctic processes and has been found insufficient to simulate snowpack properties in an Arctic environment (Woolley et al., 2024). An Arctic version of ESCROC within SVS2-Crocus (Arctic SVS2-Crocus) was

170 developed by Woolley et al. (2024) that relied on existing parameterisations that have been developed for Arctic snowpacks to overcome these limitations (Barrere et al., 2017; Lackner et al., 2022; Royer et al., 2021b; Gouttevin et al., 2018). Woolley et al. (2024) implemented new parametrisations that considered the impact of wind speed on surface snow following Royer et al. (2021b) and Lackner et al. (2022) by modifying the default parameterisation of Vionnet et al. (2012) for falling snow density. As wind speed also increases surface snow density during drifting or blowing snow events, Woolley et al. (2024) also

175 modified the parameter that modulates the increase in density for a given snow transport intensity. The maximum density of snow impacted by wind was also raised following the work of Barrere et al. (2017), Royer et al. (2021b) and Lackner et al. (2022). To consider the impact of basal vegetation on compaction and metamorphism, wind compaction was deactivated, and viscosity was increased below a set polar vegetation height (Domine et al., 2016; Gouttevin et al., 2018; Royer et al., 2021b). Finally, alternate thermal conductivity formulations better suited for Arctic snow types were implemented in Arctic SVS2-

180 Crocus (Fourteau et al., 2021; Sturm et al., 1997). Parameterising missing Arctic processes within SVS2-Crocus improved the simulation of snow density and SSA at Trail Valley Creek when compared to the default version of the model (Woolley et al., 2024). A detailed description of the options for each physical process for the default and Arctic SVS2-Crocus ensembles can be found in Woolley et al. (2024) and Lafaysse et al. (2017). We select the same 120-ensemble members used within Woolley et al. (2024) from default and Arctic SVS2-Crocus to investigate the spatial transferability of Arctic parameterisations across

185 the forest-tundra ecotone. Further recent developments of SVS2-Crocus include the implementation of a canopy module to simulate snowpack properties in forested environments. The module simulates the impact of forest canopy on near surface meteorological variables such as air temperature, wind speed, relative humidity and radiative fluxes (Mazzotti et al., 2024). The canopy module is described in Appendix A.

190 The root-mean-square error (RMSE) and spread skill (SS) were used to evaluate the simulation of snow depth, SWE, bulk density and profiles of density and SSA. The RMSE represents the accuracy of a modelled outcome in comparison to a measured result, whereas the SS measures the ratio of the root-mean ensemble spread to the RMSE of the ensemble mean against a measured result (Lafaysse et al., 2017). A SS value of 1 indicates measurements lie within the ensemble spread and represents perfect dispersion (Fortin et al., 2014). Statistics were calculated for the overall ensemble, the depth hoar fraction

195 (DHF), and the wind slab (WS) fraction by identifying transitions in the density and/or SSA of measured profiles. DHF values used within this study varied from 40 to 64 %, and all snow above the depth hoar layer was classified as wind slab. Simulated

profiles of density and SSA were classified into their vegetation type following Fig. 1 & 2 for statistical analysis as follows: Tundra (Upper Plateau and Trail Valley Creek), Deciduous Shrub (Valley, Small Shrub and Mixed Shrub) and Forest (Shrub Tree and Havikpak). As measured and simulated profiles can differ in depth and vertical resolution, all profiles were normalised and then rescaled to 0.005 increments up to the maximum depth, interpolated using layer thickness to allow for fair layer evaluation.

3.2.2 SMRT

The Snow Microwave Radiative Transfer model (SMRT; Picard et al., 2018) was used to simulate the backscatter signal following the model configuration of Montpetit et al. (2024): Ku-band (13.5 GHz) frequency, VV single-polarization, incidence angle of 40⁰, exponential microstructure model, improved born approximation (IBA) electromagnetic model, and the Discrete Ordinate and Eigenvalue (DORT) radiative transfer solver (Picard et al., 2018). Each snow layer within SMRT is characterised by temperature, density, thickness and exponential correlation length (ρ_{ex}), using either SVS2-Crocus simulations or snowpit measurements. The exponential correlation length was derived from the optical diameter (d_{opt}) and density (ρ_{snow}):

$$\rho_{ex} = \frac{2}{3} . K . \left(1 - \frac{\rho_{snow}}{\rho_{ice}}\right) . d_{opt} \tag{1}$$

where the polydispersity (K) was assumed to be 1 for all simulations (Meloche et al., 2024). Measurements of SSA were converted into d_{opt}:

$$d_{opt} = \frac{6}{\rho_{ice} . SSA} \tag{2}$$

Effective soil permittivity (2.7) and effective soil roughness (0.011) values used for Trail Valley Creek in Montpetit et al. (2024) were applied to all sites in this study. SMRT simulations of radar backscatter used vertical profiles of snowpack properties simulated by 120-members of default and Arctic SVS2-Crocus (see section 3.2.1 for a description of ensemble members) from the date of measurement during the 2021/22 and 2022/23 field campaigns. Initial simulations were run with a multi-layer snowpack (~ 20 layers) to investigate the impact of detailed snow microstructure on the backscatter signal. The multi-layer snowpack was then simplified into a 3-layer radar equivalent snowpack using a K-means clustering algorithm following the methods of Meloche et al. (2024). The method aims to increase the computational efficiency needed for SWE retrieval whilst conserving the bulk SWE and microwave scattering behaviour of the snowpack. In addition, two techniques were applied to the SVS2-Crocus multi-layer and simplified snowpack SMRT simulations to optimize the scattering behaviour of the snowpack. Firstly, a vertically averaged scaling factor of 0.63 (Brucker et al., 2011) was applied to each layer of SVS2-Crocus simulated profiles. Secondly, a minimum SSA of 8.7 m² kg⁻¹ (maximum d_{opt} of 0.75 mm) was applied to each layer

of SVS2-Crocus simulated profiles. Analysis of pit measurements found 8.7 m^2 kg^{-1} to be the median minimum value across
230 all sites used within this study for both 2021/22 and 2022/23, and lies within the range of depth hoar SSA measurements made
across the wider Arctic (Woolley et al., 2024; Rutter et al., 2019; Montpetit et al., 2024).

4.0 Results

4.1 Bulk Snow Properties: SWE, Snow Depth and Density

Measured snow depth and SWE increased southward across the forest-tundra ecotone during the winters of 2021/22 and
235 2022/23. The shallowest snow depths were found at TVC (0.41 m; 2022) and Valley (0.4 m; 2023) and the deepest at Shrub
Tree (0.72 m; 2022 and 0.69 m; 2023). Valley (95 kg m^{-2}; 2022) and Small Shrub (84 kg m^{-2}; 2022) exhibited the lowest
measured SWE whereas Shrub Tree consistently exhibited the highest measured SWE across both years (162 kg m^{-2}; 2022 and
153 kg m^{-2}; 2023). Measured bulk density decreased southward across the ecotone with highest bulk density values at TVC
(293 kg m^{-3}; 2022 and 334 kg m^{-3}; 2023) and lowest at Havikpak (191 kg m^{-3}; 2022) and Mixed Shrub (198 kg m^{-3}; 2023).
240 Deeper snow depths and higher SWE were found in 2022 than 2023 for all sites due to higher snowfall early in the snow
season in 2022 (Fig. 3) whereas bulk density was higher in 2023 than 2022.
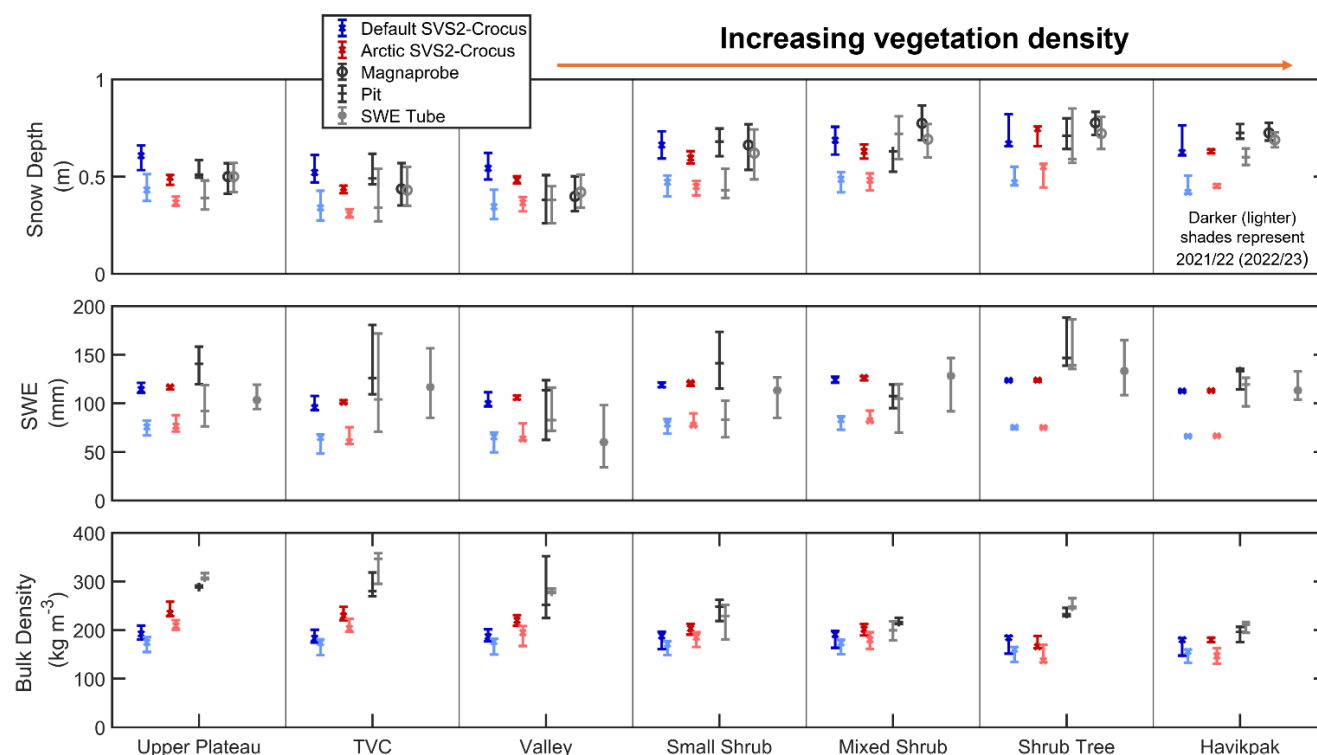
Figure 4: Distribution (median, interquartile range) of simulated and measured snow depth (m), SWE (kg m^{-2}) and bulk density (kg m^{-3}) at each site for the 2021/22 and 2022/23 winter. Lighter shades of each colour represent the winter of 2022/23. Each distribution represents simulated and measured snow properties at the time of snowpit measurements. Vegetation type for each site is described in Fig. 1.

Both default and Arctic SVS2-Crocus driven by HRDPS are able to simulate the measured increase in snow depth that occurs along the transition zone from tundra to forest (Fig. 4). Deepest snow depths (Fig. 4; mean across 2021/22 and 2022/23: 0.61 m) simulated at Shrub Tree due to high snowfall and canopy cover restricting wind compaction and redistribution show good agreement with measurements in 2021/22 (default RMSE: 0.08 m; Arctic RMSE: 0.05 m) and underestimation in 2022/23 (default RMSE: 0.13 m; Arctic RMSE: 0.12 m). Shallowest snow depths are simulated at TVC (Fig. 4; mean across 2021/22 and 2022/23: 0.37 m) due to lower snowfall and exposure to high winds in both 2021/22 (default RMSE: 0.11 m; Arctic RMSE: 0.06 m) and 2022/23 (default RMSE: 0.09 m; Arctic RMSE: 0.04 m).

Wind effect modifications applied to Arctic SVS2-Crocus lead to higher simulated bulk densities and shallower snow depths at all sites when compared to default SVS2-Crocus (Fig. 4). Arctic SVS2-Crocus simulated bulk density was highest at Upper Plateau (2022: 241 kg m^{-3}) and TVC (2023: 234 kg m^{-3}) due to high wind speeds resulting from exposed topography whereas default SVS2-Crocus simulated lowest bulk densities at Havikpak (2022: 171 kg m^{-3}; 2023: 150 kg m^{-3}) due canopy cover reducing wind speed and compaction processes. As both default and Arctic SVS2-Crocus received identical precipitation

260   forcing from the HRDPS, they simulate similar magnitudes of SWE (Fig. 4). Default and Arctic SVS2-Crocus show good
       agreement with measurements for the simulation of SWE at all sites in 2021/22 (Fig. 4; default RMSE range: 12 – 28 kg m^{-2};
       Arctic RMSE range: 8 – 25 kg m^{-2}). However, SWE is underestimated by both ensembles at TVC (default RMSE: 51 kg m^{-2};
       Arctic RMSE: 46 kg m^{-2}), Shrub Tree (default and Arctic RMSE: 61 kg m^{-2}) and Havikpak (default RMSE: 50 kg m^{-2}; Arctic
       RMSE: 50 kg m^{-2}) in 2022/23. The differences in snow depth simulated by default and Arctic SVS2-Crocus therefore result
265   from the opposing trends in bulk density (Fig. 4).

4.2 Profiles of density and SSA

Figures 5 and 6 compare measured and simulated profiles of snow density and SSA for 3 sites of contrasting vegetation types
(tundra: Upper Plateau, deciduous shrubs: Small Shrub and forest: Havikpak – as defined in section 3.2.1) for the 2021/22 and
2022/23 winter seasons, respectively. All remaining sites are displayed in Appendix B. Measured profiles of snow density at
270   tundra and deciduous shrub sites exhibit the typical structure of an Arctic snowpack: low-density basal layers ranging between
       150 kg m^{-3} and 300 kg m^{-3} overlain by higher density surface layers ranging between 300 kg m^{-3} and 400 kg m^{-3} (Fig. 5 & 6,
       Appendix B). At forest sites, measured snow density shows less variability throughout the snowpack with surface and basal
       layers exhibiting similar densities (Fig. 5 & 6, Appendix B: WS Mean: 196 kg m^{-3}; DHF Mean: 192 kg m^{-3}). Despite differences
       in snow density, the pattern of measured SSA is consistent amongst all sites with lower SSA values for basal layers (ranging
275   between 5 m^2 kg^{-1} and 20 m^2 kg^{-1}) and higher SSA (ranging between 30 m^2 kg^{-1} and 60 m^2 kg^{-1}) values for near-surface layers
       (Fig. 5 & 6, Appendix B). The variability between measured pit profiles of density and SSA decreases from tundra to forest
       (Fig. 5 & 6, Appendix B).
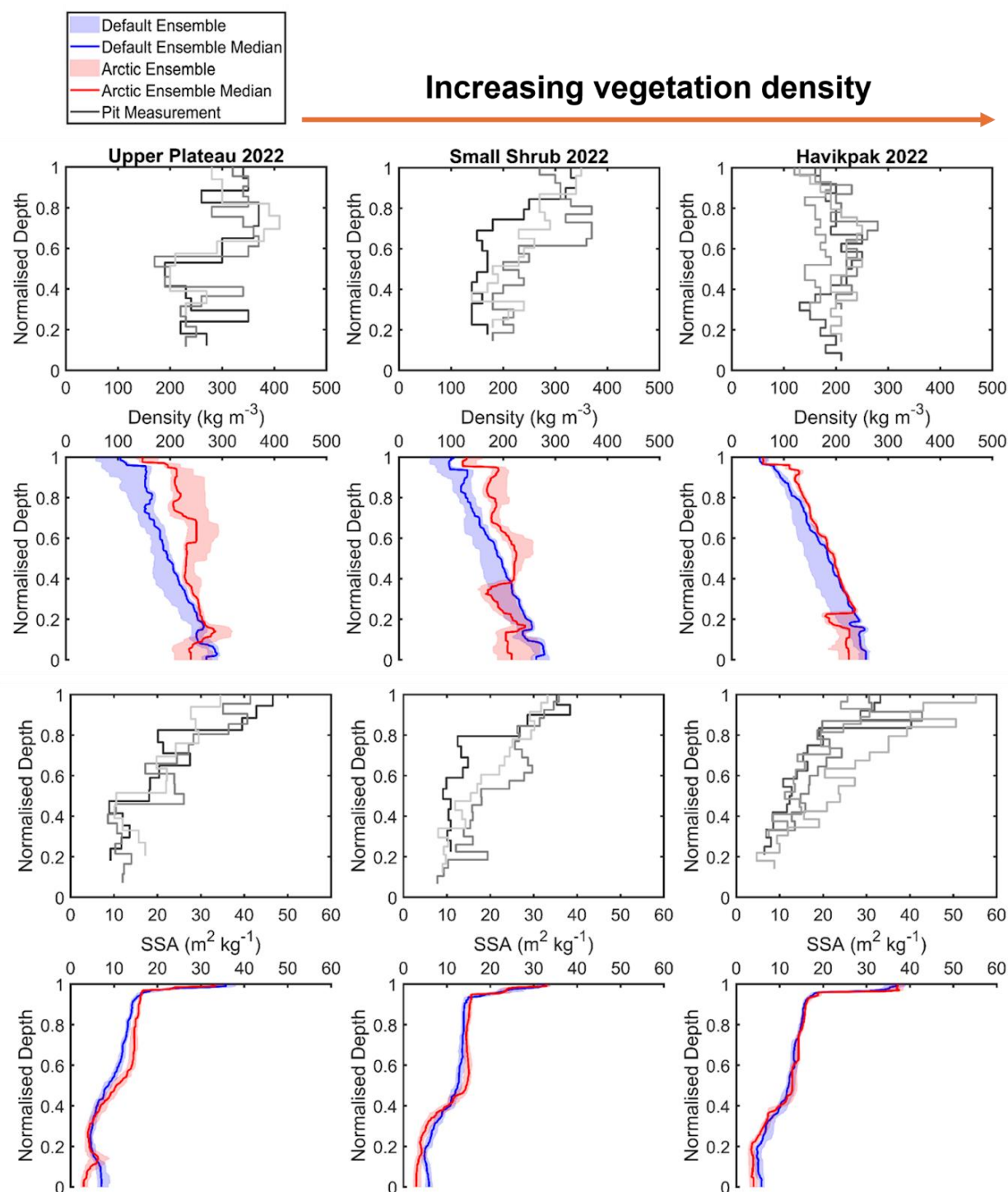
280 **Figure 5:** Comparison of measured and simulated vertical profiles of density (kg m^{-3}, median, interquartile range) and SSA (m^2 kg^{-1}, median, interquartile range) by default and Arctic SVS2-Crocus from the March 2022 winter field campaign. Black and grey lines indicate different pit profiles. Vegetation type for each site is described in Fig. 1.
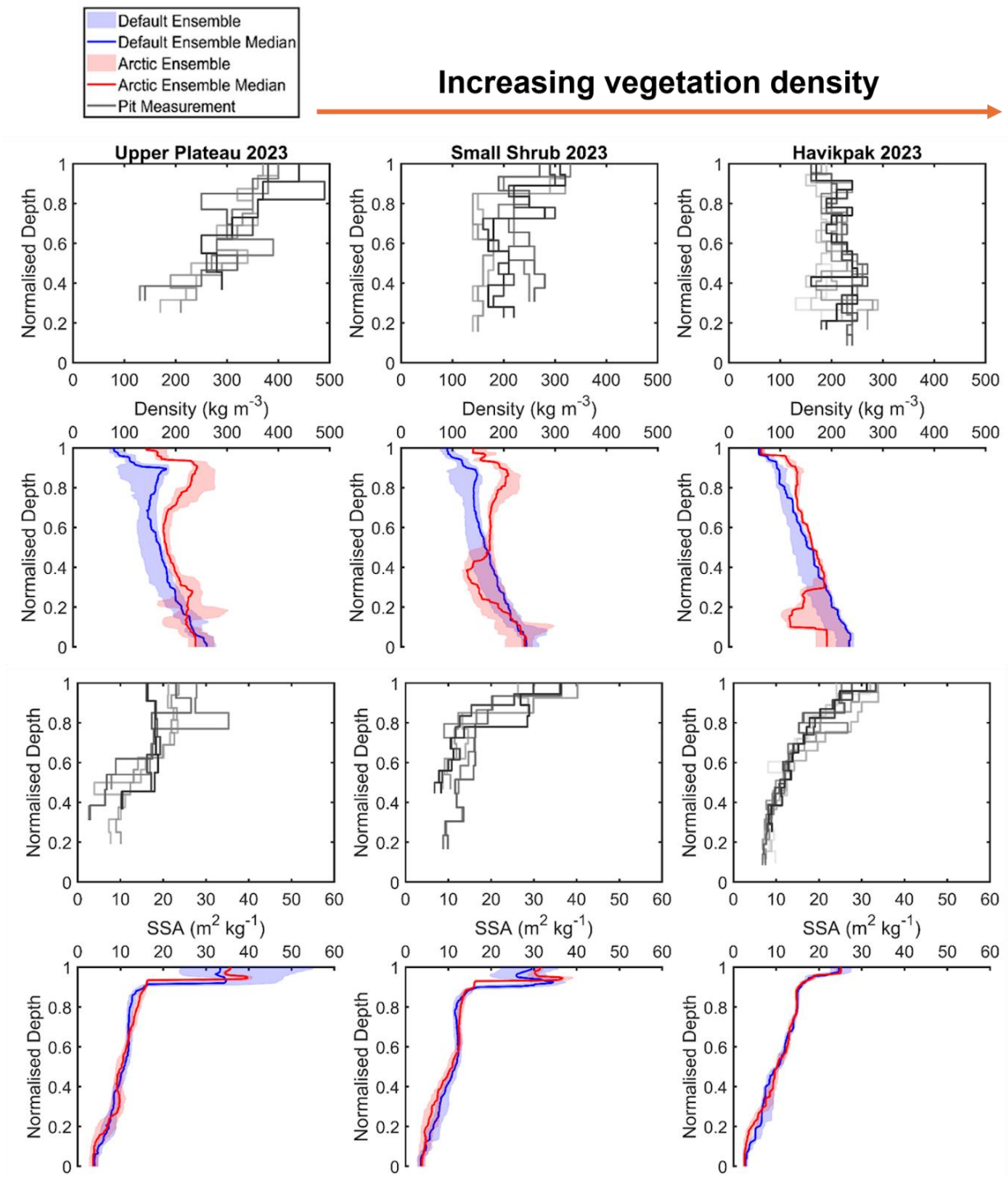
Figure 6: Comparison of measured and simulated vertical profiles of density (kg m⁻³, median, interquartile range) and SSA (m² kg⁻¹, median, interquartile range) by default and Arctic SVS2-Crocus from the March 2023 winter field campaign. Black and grey lines indicate different pit profiles. Vegetation type for each site is described in Fig. 1.

At all sites, for both winter seasons, default SVS2-Crocus underestimates surface layer density (Fig. 7: 2022 & 2023: tundra RMSE: 202 kg m^{-3}; deciduous shrubs RMSE: 141 kg m^{-3}; forest RMSE: 106 kg m^{-3}). Wind effect parameterisations applied to Arctic SVS2-Crocus are effective in compacting surface snow layers, reducing the RMSE at all sites (Fig. 7: 2022 & 2023:

290   tundra RMSE: 138 kg m^{-3}; deciduous shrubs RMSE: 97 kg m^{-3}; forest RMSE: 84 kg m^{-3}). The performance of the Arctic parameterisations are most effective at tundra and deciduous shrub sites where high wind speeds contribute to a significant proportion of surface snow compaction. At forest sites, the parameterisation of below-canopy wind speed reduces the ability of Arctic parameterisations to compact surface layers resulting in a smaller reduction in RMSE. Despite improvements in the RMSE by Arctic SVS2-Crocus, surface snow density is underestimated at all sites (Fig. 5, 6 & Appendix B). This remaining

295   underestimation is likely due to uncertainties associated with wind speed within the HRDPS meteorological forcing data. The spread of the Arctic SVS2-Crocus ensemble (Fig. 7: 2022 & 2023: tundra SS: 0.34; deciduous shrubs SS: 0.54; forest SS: 0.38) captures the variability in snow pit measurements better than default SVS2-Crocus (Fig. 7: 2022 & 2023: tundra SS: 0.19; deciduous shrubs SS: 0.27; forest SS: 0.30) but both ensembles display under dispersion (SS < 1). The spread of both ensembles decreases from tundra to forest, similar to patterns observed within measurements (Fig. 7).

300
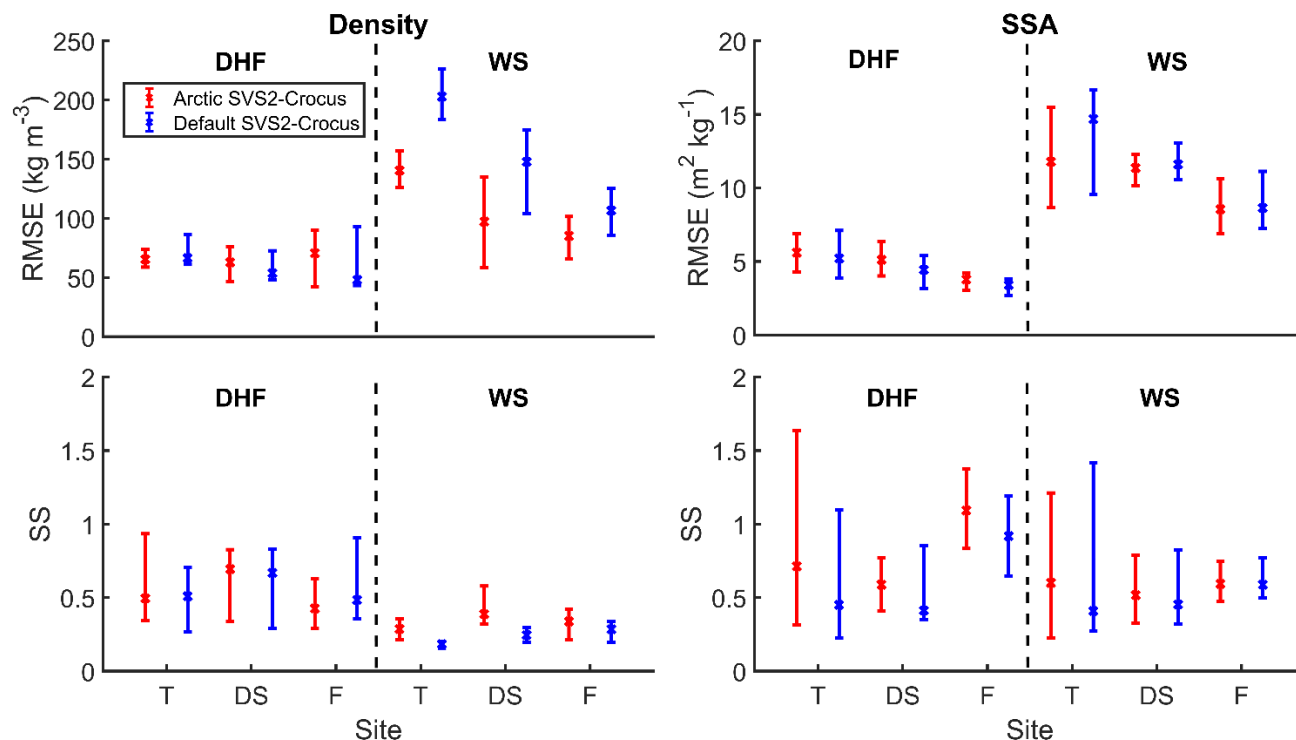
Figure 7: RMSE and SS scores the simulation of density (kg m^{-3}) and SSA (m^2 kg^{-1}) by default and Arctic SVS2-Crocus for different vegetation types (T: Tundra; DS: Deciduous Shrubs: F: Forest – described in section 3.2.1) for the 2021/22 and 2022/23 field campaigns.
305   Scores are separated for depth hoar and wind slab.

Simulated basal layer densities by default and Arctic SVS2-Crocus range from ~150 kg m^{-3} to ~250 kg m^{-3} and are often too low in comparison to measurements. The RMSE of default SVS2-Crocus (Fig. 7; deciduous shrubs RMSE: 63 kg m^{-3}; forest RMSE: 71 kg m^{-3}) for the simulation of basal layer density is lower than that of Arctic SVS2-Crocus (Fig. 7; deciduous shrubs RMSE: 67 kg m^{-3}; forest RMSE: 80 kg m^{-3}) at deciduous shrub and forest sites for the 2021/22 and 2022/23 winters. Arctic

310 SVS2-Crocus reduces the error at tundra sites (Fig. 7; default tundra RMSE: 72 kg m^{-3}; Arctic tundra RMSE: 66 kg m^{-3}). The parameterisations applied to Arctic SVS2-Crocus work to decrease basal layer density but are not effective in improving the overall error (Fig. 7). The compaction parameterisation within default SVS2-Crocus that simulates a profile of increasing density with snow depth results in basal densities that are in some cases similar to Arctic SVS2-Crocus despite the large underestimation in surface layer density (Fig. 5, 6 & 7, Appendix B). The SS of the Arctic SVS2-Crocus ensemble better

315 captures the variability in measurements than of default SVS2-Crocus at forest sites (Fig. 6; default SS: 0.71; Arctic SS: 0.80). Similar SS scores are observed at tundra sites (Fig. 7; default SS: 0.62; Arctic SS: 0.63) and an improvement using default SVS2-Crocus is found at forest sites (Fig. 7; default SS: 0.77; Arctic SS: 0.57).

Both default and Arctic SVS2-Crocus underestimate surface and basal layer SSA. Simulated SSA increases towards the

320 surface, reaching a maximum value of 38 m^2 kg^{-1} at Havikpak in March 2022, likely due to fresh snowfall and a reduced rate of wind-induced compaction resulting in lower density surface snow (Fig. 5 & 6, Appendix B). Arctic parametrisations contribute to a minor increase in the RMSE (Fig. 7; 2022 & 2023: tundra RMSE: 6 m^2 kg^{-1}; deciduous shrubs RMSE: 5 m^2 kg^{-1}; forest RMSE: 4 m^2 kg^{-1}) in simulated basal layer SSA at all sites in comparison to default SVS2-Crocus (Fig. 7; 2022 & 2023: tundra RMSE: 5 m^2 kg^{-1}; deciduous shrubs RMSE: 4 m^2 kg^{-1}; forest RMSE: 3 m^2 kg^{-1}). Both ensembles have similar

325 error for simulation of surface layer SSA (Fig. 7; 2022 & 2023: tundra RMSE: 12.5 m^2 kg^{-1}; deciduous shrubs RMSE: 11 m^2 kg^{-1}; forest RMSE: 9 m^2 kg^{-1}). Arctic SVS2-Crocus (Fig. 7; 2022 & 2023: tundra SS: 0.93; forest SS: 0.93) better captures the variability in basal layer SSA than default SVS2-Crocus at tundra and deciduous shrub sites (Fig. 7; 2022 & 2023: tundra SS: 0.60; deciduous shrubs SS: 0.79), due to greater ensemble spread. Default SVS2-Crocus (Fig. 7; default SVS2-Crocus 2022 & 2023: tundra SS: 0.83; forest SS: 0.78) exhibits greater skill in capturing variability in surface layer SSA at tundra and forest

330 sites (Arctic SVS2-Crocus 2022 & 2023: tundra SS: 0.72; forest SS: 0.76) than at deciduous shrub. Simulated profiles of SSA exhibit a narrow spread in comparison to that of the measured profile, suggesting that the uncertainty in the metamorphism scheme is underestimated within SVS2-Crocus.

335

4.3 Simulated Ku-band backscatter

The exponential microstructure model, used within SMRT to compute the scattering coefficient, characterizes snow

340 microstructure using the exponential correlation length which can be derived from SSA and density (Eq. 1; Picard et al., 2018). As Arctic parameterisations work to modify both SSA and density and since Ku-band frequency is highly sensitive to the snow grain size (Lemmetyinen et al., 2014), we investigate the impact of SSA and density on a) the exponential correlation length (Fig. 8) and b) the resulting snow backscatter (Fig. 9). Small errors in simulated basal SSA, which is underestimated by both default and Arctic SVS2-Crocus result in large errors in the optical diameter and in the exponential correlation length (Fig. 8).

345 Low basal SSA values result in a correlation length that is too long (0.6×10^{-3} - 0.8×10^{-3} m) for the base of the snowpack in comparison to measurements (0.2×10^{-3} m). Errors in the simulation of surface layer SSA result in smaller errors in the exponential correlation length for the surface of the snowpack (Fig. 8). By substituting small simulated basal SSA values with larger snowpit measurements of SSA, the simulated exponential correlation length is shorter (0.2×10^{-3} - 0.3×10^{-3} m).

350
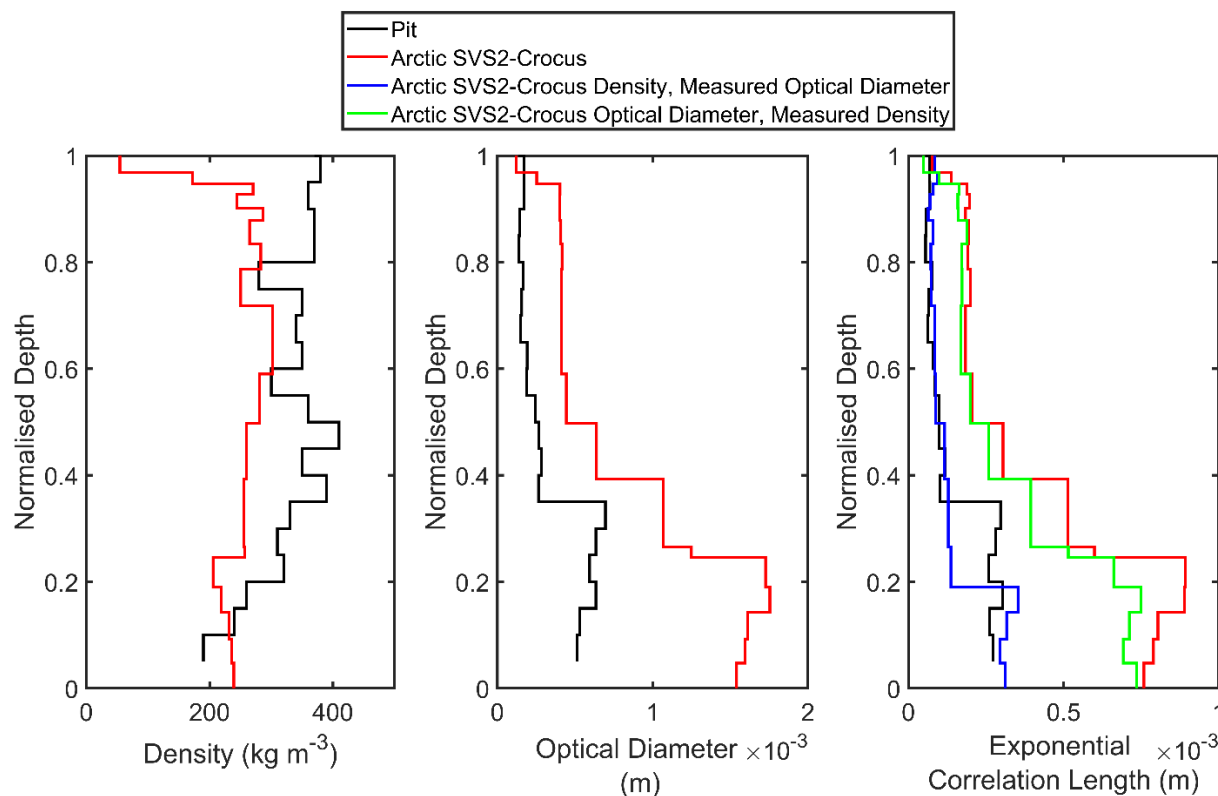
Figure 8: Impact of density and optical diameter on the exponential correlation length at TVC (2021/22) simulated by Arctic SVS2-Crocus (Eq.1).
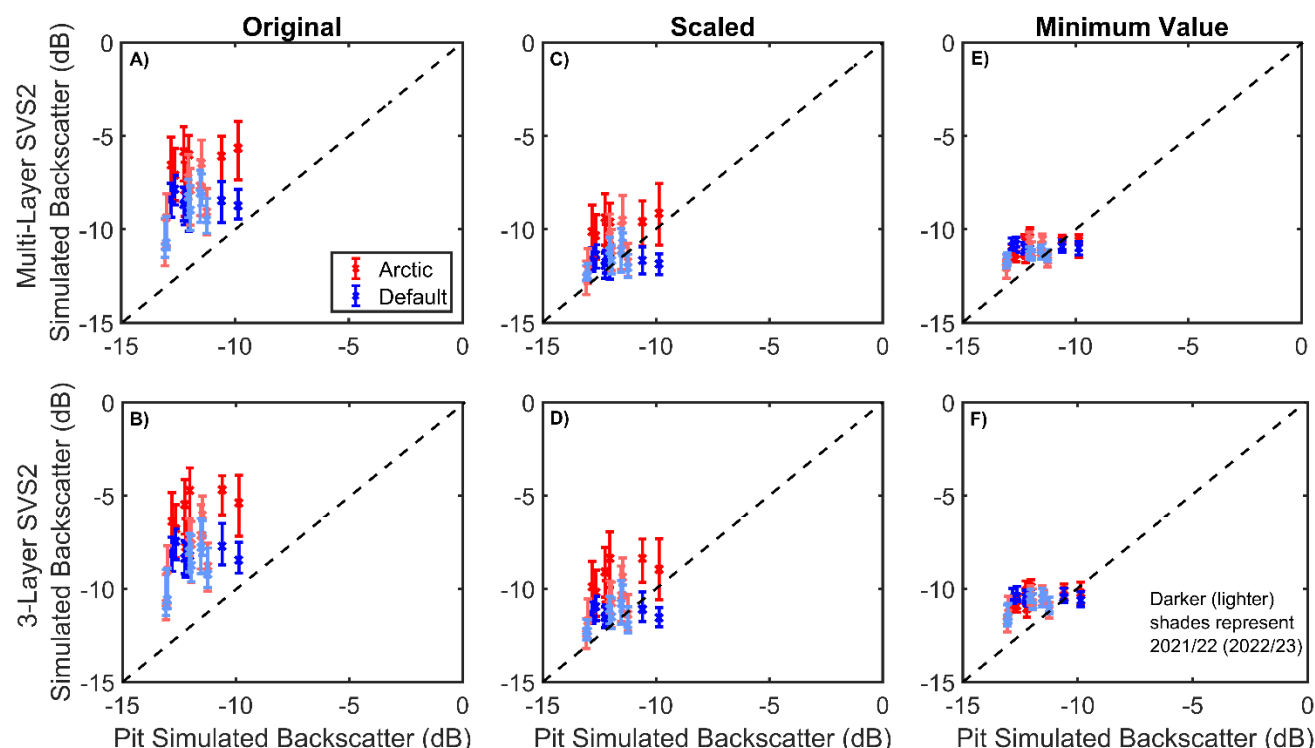
Figure 9: Comparison between pit simulated backscatter and SVS2-Crocus simulated backscatter for a multi-layer (A, 'Original') and 3-layer (B, 'Original') radar equivalent snowpack (interquartile range, median) for the 2021/22 and 2022/23 winter seasons at Ku-band frequency (13.5 GHz). C & D) comparison using a SSA scaling factor of 0.63 ('Scaled') and E & F) comparison with a minimum SSA of 8.7 m^2 kg^{-1} ('Minimum Value'; maximum optical diameter equivalent 0.75 mm).

Figure 9 compares two sets of backscatter simulations at Ku-band frequency (13.5 GHz). The first set of simulations uses snow pit measurements as inputs to SMRT ('Pit Simulated Backscatter' in Fig. 9). The second set of simulations uses simulated snowpack properties from default and Arctic SVS2-Crocus as inputs to SMRT ('Multi-Layer/3-Layer SVS2 Simulated Backscatter' in Fig. 9). The error in simulated backscatter is greater when using Arctic SVS2-Crocus due to a larger underestimation in basal SSA which results in an overestimation of the exponential correlation length and increased scattering. Across all sites, pit simulated backscatter varies from -5.9 dB to -14.3 dB whereas SVS2-Crocus simulated backscatter varies from -2.7 dB to -13.4 dB (Fig. 9). Both default and Arctic SVS2-Crocus overestimate backscatter (Fig. 8; ranging from -5 to -10 dB) in comparison to simulated backscatter using snowpit measurements (Fig. 9; ranging from -10 to -14 dB). The RMSE when using default SVS2-Crocus is greatest at Upper Plateau (mean RMSE: 5.0 dB) whereas the RMSE for Arctic SVS2-Crocus is greatest at sites Mixed Shrub and Shrub Tree (mean RMSE 6.6 dB). At Small Shrub and Shrub Tree, the difference in simulated basal SSA between default and Arctic SVS2-Crocus exceeds that of other sites (Fig. 5 & 6, Appendix B), leading to no overlap in ensemble ranges for backscatter simulation (Fig. 9), highlighting the impact of basal SSA errors.

Table 1: Mean RMSE between simulated SVS2-Crocus backscatter and snowpit simulated backscatter (dB) for all seven sites for the 2021/22 and 2022/23 winter seasons. Separated for default and Arctic SVS2-Crocus. Letters refer to panels on Fig. 9.

	2022		**2023**	
	Arctic	Default	Arctic	Default
A) SVS2 Original	5.3	3.5	4.2	3.6
B) 3-Layer Original	5.8	3.9	4.6	3.9
C) SVS2 Scaled	2.7	1.6	2.4	1.8
D) 3-Layer Scaled	2.6	1.7	2.5	1.8
E) SVS2 Minimum	1.3	1.4	1.6	1.5
F) 3-Layer Minimum	1.7	1.7	2.0	1.9

375

As the underestimation in basal SSA values simulated by both default and Arctic SVS2-Crocus have a large impact on the simulation of snow backscatter, we investigated two methods to reduce this error. Method one reduces the scattering behaviour of the snow grains with a vertically averaged scaling factor of 0.63 (Brucker et al., 2011; Fig. 9c & 9d). The second method

380 limits the minimum SSA of the snow grains to a value of 8.7 m^2 kg^{-1} (average median DHF value from all pit measurements at all sites) to remove the impact of unrealistically low simulated values (Fig. 9e & 9f). By reducing the scattering effect of the snow grains which results in a weaker backscatter (values ranging from -8 to -13 dB), the vertically averaged scaling is effective in reducing the error in the simulation by both default and Arctic SVS2-Crocus for a multi-layer snowpack (Table 1c).

385 Implementing a minimum SSA value removes the influence of large snow grains on the simulation of snow backscatter and allows the simulation of a weaker backscatter that is more representative of measurements (values ranging between -10 to -12 dB). Applying a minimum SSA value also reduces the difference between default and Arctic SVS2-Crocus suggesting this method constrains a key model uncertainty that contributes towards the inaccurate simulation of snow backscatter (Fig. 9e & 9f; Table 1e). The average RMSE of all sites is reduced when applying a minimum value by 59% for default SVS2-Crocus

390 and 67% for Arctic SVS2-Crocus for 2021/22 and 2022/23. The reduction in the RMSE for Arctic SVS2-Crocus is greater than that of default SVS2-Crocus, suggesting the improved simulated density profile contributes to the improved simulation of backscatter when the large influence of low SSA values is removed.

A radar-equivalent snowpack is able to replicate the scattering behaviour of the multi-layer snowpack, resulting in an RMSE

395 below 1 dB (Table 1) at all sites except for Shrub Tree (RMSE: 1.32 dB) and Havikpak (RMSE: 1.30 dB) in 2022 where snowpacks are deeper and more complex than in 2023 (Fig. 4). The overestimation in simulated backscatter when compared to snowpit simulated backscatter is consistent between both multi-layer (Table 1a) and 3-layer simulations (Table 1b). Using a vertically averaged scaling factor also reduces the error for a radar-equivalent snowpack (Table 1d). Following the pattern

of the multi-layer snowpack, implementing a minimum SSA values reduce the RMSE at all sites when using a radar-equivalent

400 snowpack by 54% (default SVS2-Crocus) and 65% (Arctic SVS2-Crocus) for 2021/22 and 2022/23. The computation time in

SMRT simulations was reduced by 60% by simplifying the multi-layer snowpack (~20 layers) to a radar equivalent snowpack

(3 layers). The radar-equivalent snowpack can therefore increase the computational efficiency for SWE retrieval algorithms

without altering the scattering behaviour.

5.0 Discussion

405 Accurate simulation of profiles of snow density, and especially SSA, by physical snowpack models are crucial inputs to

radiative transfer models for accurate estimation of SWE (Derksen et al., 2021; Tsang et al., 2022). Consequently, to assess

the reliability of Ku-band backscatter SWE retrievals, an evaluation of simulated density and SSA by SVS2-Crocus was first

conducted across the forest-tundra ecotone to quantify uncertainties in the representation of physical snow properties (section

5.1). Analysis then follows of the impact uncertainties in simulated density and SSA have on the simulation of Ku-band

410 backscatter (section 5.2).

5.1 Impact of vegetation on simulated snowpack properties

Evaluation of SVS2-Crocus driven by HRDPS meteorological forcing data across the forest-tundra ecotone demonstrates that

Arctic modifications are effective in representing the impact of vegetation by reducing the error in the simulation of bulk

snowpack properties, enhancing the spatial transferability of Arctic SVS2-Crocus. Both default and Arctic SVS2-Crocus

415 simulated the observed increase in snow depth that occurs across the forest-tundra ecotone where taller shrubs and sparse

evergreen needleleaf forest canopies trap snow (Essery and Pomeroy, 2004) and reduce wind speed minimising snow

redistribution (Roth and Nolin, 2017) and compaction (Gouttevin et al., 2018) within shrubs and beneath tree canopies. At

tundra sites, where vegetation is low and wind speeds are high, Arctic modifications are effective in counteracting the

dominance of compaction due to the weight of the overlying snow within SVS2-Crocus (Vionnet et al., 2012), working to

420 decrease snow depth and increase bulk density in line with measurements (Woolley et al., 2024; Royer et al., 2021b; Lackner

et al., 2022). The addition of a canopy module within SVS2-Crocus allowed for snow-forest interactions to be simulated but

led to an underestimation in bulk density at all forested sites due to uncertainties in the HRDPS wind speed and in the

parameterisation of below-canopy wind speed. Furthermore, SVS2-Crocus does not simulate the evolution of snow properties

in the canopy due to metamorphism and classifies unloaded snow as fresh snowfall (Lumbrazo et al., 2022). Implementing a

425 parameterisation that considers the density and microstructure of snow within the canopy may reduce the underestimation in

simulated bulk density (Bouchard et al., 2024). As the sites selected for use within this study represent the edge of the forest-

tundra ecotone where forest canopies are sparse (< 15 %) and wind speed plays a role in shaping the snowpack (Derksen et

al., 2014), current parameterisations designed for dense canopies may be inappropriate for these environments.

Coupling of SVS2-Crocus and HRDPS successfully simulated snowpack properties at sites where in-situ meteorological data

430   were not available, supporting the use of the coupling within future studies and the need for such datasets for research at remote sites. Implementing wind effect modifications into Arctic SVS2-Crocus reduced the error in the simulation of surface snow density at all sites across the forest-tundra ecotone by an average of 29%. Parameterising wind-induced compaction, the impact of wind on fresh snow density, and raising the maximum density impacted by wind in surface layers, reduced the error in Arctic SVS2-Crocus simulations in comparison to default SVS2-Crocus, confirming the ability of Arctic SVS2-Crocus to

435   generate more realistic simulations of surface layer density at a wide range of sites across the forest-tundra ecotone. As Arctic SVS2-Crocus exhibits an improved ensemble dispersion (SS value closer to 1) at all sites, it suggests that the optimal skill of the Arctic parameterisations are better suited to Arctic environments when compared to default SVS2-Crocus. Although wind effect modifications work to improve the simulation of surface snow density in comparison to default SVS2-Crocus, simulated values are still underestimated when compared to measurements. Comparing Arctic SVS2-Crocus simulations at TVC using

440   in-situ meteorological data (see Fig. 6 of Woolley et al., 2024) with simulations using HRDPS forcing within this study (Appendix B), we find a 43 % increase in RMSE for surface layer density. The decreased accuracy indicates that the simulated results deviate more from observed values when relying on HRDPS meteorological forcing data, suggesting an underestimation in HRDPS wind speed and associated wind-induced compaction. At non-forested sites, the reduction in the RMSE is greater (31 %; tundra and deciduous shrubs) than at forest sites (21 %; forest) as the compaction effects of the Arctic parameterisations

445   at forested sites are inhibited by the parameterisation of below-canopy wind speed. Despite inclusion of a canopy parameterisation that incorporates a weighted average of the wind profile in open and closed environments (Mazzotti et al., 2024), the reduction in wind speed was too high for sparse canopies, reducing the rate of wind-induced compaction, leading to an underestimation in surface layer density.

450   Statistically, basal vegetation effect modifications do not improve the simulation of basal layer density when compared to default SVS2-Crocus, but modifications are necessary to simulate a physically representative density profile in an Arctic environment. Without the basal vegetation effect modifications, default SVS2-Crocus would simulate a profile of increasing density due to the dominance of compaction, which when combined with the wind effect modifications would lead to basal densities that are overestimated. The statistical analysis of basal vegetation effect modifications within this study is limited as

455   density measurements in layers close to the base of the snowpack are often impeded by shrubs. The ability to select the height of polar vegetation with Arctic SVS2-Crocus simulations is a key feature that allows for the impact of differing shrub height between sites to be represented that is not considered within default SVS2-Crocus. The polar vegetation heights selected for use within this study were similar to measurements during the March 2021/22 and 2022/23 field campaigns and represent bending of shrubs due to the weight of the overlying snow (Belke-Brea et al., 2020; Ménard et al., 2014). However, some

460   simulated profiles can be shallower than measured profiles as a function of the precipitation inputs meaning some polar vegetation heights encompass much of the simulated profile. This is particularly evident at sites Small shrub and Mixed shrub, where the selected height of polar vegetation causes the basal vegetation effect modifications to activate at greater snow depths

(Fig. 5 & 6, Appendix B). As a result, the basal vegetation effect modifications work to counteract wind-induced compaction and reduce the impact of the wind effect modifications. Future work could focus on revising the parameterisation of basal
465   vegetation modifications. Considering the effect of polar vegetation within the base of an Arctic snowpack is crucial as shrubification of the Arctic is expected with a warming climate (Sturm et al., 2001; Nill et al., 2022).

Much previous work illustrating the need for Arctic specific parameterisations for the simulation of snowpack properties has focused on improving the density profile, supporting simulations of soil temperatures and permafrost modelling (Royer et al.,
470   2021b; Lackner et al., 2022; Barrere et al., 2017; Gouttevin et al., 2018). Uncertainties in simulations of SSA highlighted within this study now push the focus towards the importance of improving parameterisations of snow metamorphism for SWE retrieval (Derksen et al., 2021; Tsang et al., 2022) and data assimilation (Larue et al., 2018). Although IceCube may overestimate measurements of SSA for depth hoar grains (Martin and Schneebeli, 2023), simulated SSA by both default and Arctic SVS2-Crocus lie outside the range of typical measurements found within the Arctic (Montpetit et al., 2024; Woolley et
475   al., 2024; Rutter et al., 2019). Uncertainties in the simulation of SSA by SVS2-Crocus could stem from the growth of depth hoar in the metamorphism scheme (Marbouty, 1980) or the optical diameter (Carmagnola et al., 2014; Libois et al., 2014; Morin et al., 2013). The parameterisation of Marbouty (1980) is not well suited to simulate the optical size of depth hoar grains and should be revised for Arctic snowpacks with strong temperature gradients. Tundra sites, TVC and Valley, experience the largest underestimation in SSA suggesting the shallow snowpacks (mean TVC SD: 0.37 m; mean Valley SD: 0.41 m) generate
480   strong temperature gradients and further increase the rate of metamorphism (Wang and Baker, 2014).

5.2 Capacity to simulate snow backscatter

Low basal layer SSA values simulated by both default and Arctic SVS2-Crocus have a large impact on modelled Ku-band backscatter. The short wavelength at Ku-band (13.5 GHz) is sensitive to the coarse and large basal snow grains simulated by SVS2-Crocus as their size is comparable to the wavelength, scattering the radar signal more effectively and enhancing the
485   backscatter signal through Mie scattering (Fung, 1994). Shallow snowpacks further enhance the effect of Mie scattering from large snow grains and reduce the available contribution to volume scattering in Arctic tundra environments (King et al., 2015; Tsang et al., 2022). This is evident at sites with shallow snow depths and the most pronounced underestimation in SSA (Valley and Upper Plateau), where the RMSE in simulated backscatter is highest. Although density is known to contribute to scattering within the snowpack by altering the ice-air interfaces (King et al., 2015), the impact on the exponential correlation length is
490   secondary to that of SSA as it does not directly influence the spatial arrangement of the snow crystals (Fig. 8; Rott et al., 2009; Tsang et al., 2022). Reducing the number of SVS2-Crocus simulated layers through the approach of Meloche et al. (2024) preserves snowpack scattering characteristics and ensures snow backscatter simulations are reproduced within 1 dB accuracy. A 60% increase in computational gain using the radar-equivalent snowpack suggests that this approach can effectively increase the computational efficiency needed for SWE retrieval algorithms.

495

An improved simulation of snow backscatter can be achieved by optimizing the SSA of snow grains with a scaling factor of 0.63 or by implementing a minimum SSA value of 8.7 m^2 kg^{-1}. Both options work to reduce the scattering effects of the snowpack. As implementing a minimum SSA value removes the influence of large snow grains and constrains a key model uncertainty, it is recommended that this approach is implemented to constrain the uncertainty in simulated backscatter. The scaling factor of 0.63 accounts for the bias in SSA but also for the polydispersity of the snow grains that was set at a constant value of 1 within this study. Typical polydispersity values based upon measurements in tundra snow range from 0.6 - 0.75 for rounded grains and 1.1 - 1.9 for depth hoar (Montpetit et al., 2024; Picard et al., 2022; Sandells et al., 2024), which relate to the two-layer nature of an Arctic snowpack (Derksen et al., 2014). However, few studies have applied a polydispersity parameter to modelled output, where typical Arctic depth hoar polydispersity (1.1 - 1.9) values amplify the influence of larger simulated snow grains (low SSA/high optical diameter), shortening the exponential correlation length and increasing scattering. Before accounting for polydispersity in SVS2-Crocus, the SSA must be accurately estimated. The vertically averaged value of 0.63 proposed by Brucker et al. (2011) was successful in reducing the scattering behaviour of the SVS2-Crocus simulated snowpack, by compensating for the bias in SSA, resulting in a weaker backscatter and a reduction in the RMSE. Although based upon measurements of snow in Quebec where the depth hoar percentage is much lower than that of the Arctic, as the value is vertically averaged it is believed to compensate for the observed differences in both wind slab and depth hoar. It is also one of the only documented values that has been directly applied to Crocus output.

Implementing a minimum SSA value further reduces the error in the simulation of backscatter by both default and Arctic SVS2-Crocus by directly reducing the grain size and scattering effect of the snowpack, resulting in a weaker backscatter that is more representative of measurements. Although reducing the scattering effect of large snow grains allows density to contribute to the simulation of backscatter, basal vegetation effect modifications do not improve basal layer density, resulting in backscatter simulations remaining similar for both default and Arctic SVS2-Crocus. The spread of simulated backscatter with a minimum SSA value exhibits less variability compared to pit simulated backscatter. As the SVS2-Crocus simulated SSA and density profiles (Fig. 5 & 6) show less variability than measured profiles, removing values below 8.7 m^2 kg^{-1} further reduces the variability, making the SVS2-Crocus spread appear flatter relative to the pit simulated backscatter. However, as the variability in backscatter for both the default and Arctic SVS2-Crocus ensemble is reduced by reducing the scattering effects of the snowpack at all sites, it is suggested that the impact of low SSA values on the simulation of snow backscatter are greater than the snow model uncertainty due to parameterisation of snow processes captured by default and Arctic SVS2-Crocus (Woolley et al., 2024; Lafaysse et al., 2017). Furthermore, addressing uncertainties that contribute to an inaccurate simulation of SSA will reduce the error in the simulation of snow backscatter (Carmagnola et al., 2014; Libois et al., 2014) and will enable better estimates of snow microstructure properties for accurate retrieval of SWE (Derksen et al., 2021; Larue et al., 2018).

6.0 Conclusion

Through evaluation of the simulation of snowpack properties at 7 sites across the forest-tundra ecotone for two winter seasons
530 (2021/22 & 2022/23), the spatial transferability of Arctic SVS2-Crocus from Woolley et al (2024) driven by HRDPS
meteorological forcing has been assessed. Implementing wind effect modifications in Arctic SVS2-Crocus improves the
simulation of surface snow density at all sites across the forest-tundra ecotone and contributes to an improved simulation of
snow depth and bulk density by capturing the effects of wind-induced compaction. Simulations at sites with no forest canopy,
tundra and deciduous shrub, yield the largest reduction in the RMSE (31 %) of surface snow layers as wind speed is a dominant
535 driver in the formation of wind slab snow layers. The addition of a forest canopy module within SVS2-Crocus allows for the
simulation of snow-forest interactions which is an important feature for large-scale simulations that include forested
environments. Despite this, the parameterisation of below-canopy wind speed inhibits the ability of the wind effect
modifications to compact the surface layers of the snowpack and should be revised for areas of low canopy density (< 20 %),
where wind speed plays a large part in compacting surface layers.

540

The basal vegetation effect modifications do not statistically improve the simulation of low-density basal layers but are
necessary to simulate a physically representative Arctic density profile without parameterisation of water vapour flux. The
ability to dynamically change the height of polar vegetation is a key feature of Arctic SVS2-Crocus, not available in default
SVS2-Crocus, which represents the impact of polar low vegetation (shrubs) on basal layer density. Both default and Arctic
545 SVS2-Crocus underestimate basal and surface layer SSA at all sites across the forest-tundra ecotone in comparison to
measurements due to uncertainties in the metamorphism scheme which should be revised for Arctic environments. Expansion
of shrubs and increased vegetation density across the Arctic is projected (Mekonnen et al., 2021; Ernakovich et al., 2014) and
so the ability to simulate the impact of changing vegetation on snowpack properties using Arctic SVS2-Crocus is important to
understand future impacts of climate change in a rapidly warming region.

550

Scaling the scattering effect of snowpack microstructure by applying a scaling factor of 0.63 or implementing a minimum SSA
(8.7 $m^2 kg^{-1}$) improved the simulation of snow backscatter at Ku-band frequency at all sites across the forest-tundra ecotone.
The simulation of snow backscatter was found to be highly sensitive to low simulated SSA values leading to large errors and
an overestimation in backscatter when compared to backscatter simulations initialized with snow pit measurements. This is in
555 part due to the sensitivity of Ku-band to snowpack properties in basal layers, but also due to uncertainties in the SVS2-Crocus
snow metamorphism scheme. The ability to provide an improved simulation of backscatter using the coupling of SVS2-Crocus
and SMRT is a requirement to SWE retrieval algorithms for potential future radar missions. Reducing the number of SVS2-
Crocus simulated layers through the approach of Meloche et al. (2024) retained the scattering behaviour of the snowpack and
produced an accurate simulation of snow backscatter that was within 1 dB of the multi-layer snowpack, contributing to a
560 reduction in computational complexity (60 %) for SWE retrieval. As satellite remote sensing is our only means to monitor

SWE at continental scales, improvements to simulation of snow SSA and Ku-band backscatter progress our capacity to retrieve SWE from satellites, which will be crucial for understanding the impact of climate change in seasonally snow-covered environments.

565 **Appendix A:** The canopy module in SVS2-Crocus

The canopy module within SVS2-Crocus includes two options to represent the canopy energy balance: (i) a one-layer module similar to the module available in the FSM2 model (Mazzotti et al., 2020b; Essery et al., 2024) and (ii) a zero-layer module relying on meteorological transfer functions by means of which above-canopy meteorological data are modified to represent sub-canopy meteorological states (Ellis et al., 2010; Strasser et al., 2024). Mazzotti et al. (2024) used the zero-layer approach

570 to couple FSM2 with Crocus to simulate snowpack properties in forested environments. This approach is used in our study and is described in this appendix.

Canopy in SVS2-Crocus is defined by three structure parameters: (i) canopy height (h_{top}), (ii) canopy closure (V_{dens}) and (iii) average vegetation area index (*VAI*) of trees composing the canopy. *VAI* includes leaves, stems, and branches, and is expressed as

575 a one-sided leaf area per unit ground area of closed forest. The product $V_{dens}VAI$ converts the *VAI* per unit ground of closed forest to an effective *VAI* per unit ground of canopy that accounts for closure. The skyview factor of the canopy (*SVF*) is derived from V_{dens} and *VAI* (Essery et al., 2008):

$$SVF = \exp\left(-V_{dens}\Omega VAI\right) \tag{1}$$

580 where Ω is a clumping parameter that accounts for leaves being vertically stacked in a canopy (Essery et al., 2008; Musselman et al., 2015). Ω depends on the type of trees. In SVS2-Crocus, it is taken equal to 0.5 as proposed by Bartlett et al. (2006) for needle-leaf trees. When applied in point-scale mode, h_{top} and V_{dens} are provided by the model user as detailed on Fig. 1 for this study. *VAI* is derived from a look-up table as a function of the vegetation type specified by the user.

585 The presence of canopy in SVS2-Crocus modifies the energy and mass fluxes received by the snowpack below the canopy. The zero-layer approach assumes that canopy temperature is equal to air temperature (T_a) (Rutter et al., 2023). The longwave and shortwave radiation received at the surface below the canopy can be expressed as:

$$LW_{bv} = LW_{in}\tau_{dif} + \left(1 - \tau_{dif}\right)\sigma T_a^4 \tag{2}$$

590 $$SW_{bv} = SW_{dir}\tau_{dir} + SW_{dif}\tau_{dif} \tag{3}$$

with LW_{in} the longwave radiation above the canopy (W m^{-2}) and SW_{dir} and SW_{dif} the direct and diffuse shortwave radiation above the canopy. τ_{dif} the transmissivity of diffuse radiation through the canopy is equal to the skyview factor (e.g. Musselman et al., 2015) and τ_{dir} is the direct transmissivity of shortwave radiation defined as in Pomeroy and Dion (1996).

$$\tau_{dir} = e^{-k_{ext}V_{dens}VAI\Omega/\sin(\theta)} \tag{4}$$

where k_{ext} is an extinction coefficient taken equal to 0.5 for randomly oriented canopy elements and θ is the solar angle (rad).

Turbulent fluxes of sensible and latent heat above the snow surface below canopy are computed using wind speed, air temperature and specific humidity taken at a below-canopy reference level, h_{bc} (set to 1.5 m). Air temperature and specific humidity are taken directly from the meteorological forcing at the same height. For the wind speed, the canopy modifies the wind profile close to the surface and affects turbulent exchanges between the snow surface below the canopy and the atmosphere. As in Mazzotti et al. (2024), the wind speed below the canopy, U_{bc}, accounts for canopy closure and is taken as a weighted average of the wind speed in open terrain (unperturbed by the canopy), U_{opn}, and the wind speed below dense canopy, U_{dc}:

$$U_{bc}(h_{bc}) = (1 - V_{dens}^{0.5}) U_{opn}(h_{bc}) + V_{dens}^{0.5} U_{dc}(h_{bc}) \tag{5}$$

The wind profile in the dense canopy is assumed to be logarithmic above the canopy and exponential within the canopy:

$$U_{bc}(h_{bc}) = U_{top} \exp\left[w_{can}\left(\frac{h_{bc}}{h_{top}} - 1\right)\right] \text{ with } U_{top} = U_a \ln\left(\frac{z-d}{z_{0mv}}\right)\left[\ln\left(\frac{z_U-d}{z_{0mv}}\right)\right]^{-1} \tag{6}$$

where h_{top} is canopy height (m), U_a is wind speed (m s^{-1}) at the forcing height z_U (m) (above the ground, $z_U > h_{top}$), U_{top} is wind speed at the top of the canopy (m s^{-1}), z_{0mv} is momentum roughness length of the canopy (m) and d is the zero plane displacement height (m). z_{0mv} and d depend on the canopy height following: $z_{0mv} = 0.1h_{top}$ and $d = 0.67h_{top}$. The factor w_{can} characterizes attenuation of wind speed in the dense canopy and depends on canopy structure with $w_{can} = \beta\Omega VAI$, with $\beta = 0.9$ as in Liston and Elder (2006). In addition to the turbulent fluxes, U_{bc} is also used in SVS2-Crocus to compute properties of falling snow, wind-induced compaction and mass loss due to blowing snow sublimation for the snowpack below the canopy. SVS2-Crocus simulates snow interception by the canopy using the method of Hedstrom and Pomeroy (1998). The amount of snowfall intercepted by the canopy, I_{sv} (kg m^{-2} s^{-1}), is computed as:

$$I_{sv} = (S_{nv}^{max} - S_{nv})/\Delta t (1 - \exp(-V_{dens}SR\Delta t/W_{sv}^{max})) \tag{7}$$

where SR is the snowfall rate (kg m^{-2} s^{-1}), S_{nv} is the intercepted snow mass (kg) and S_{nv}^{max} is the maximum snow holding capacity of the canopy. S_{nv}^{max} varies with air temperature (T_a, °C) as in Andreadis et al. (2009):

$$S_{nv}^{max} = \begin{cases} 4m_{scap}V_{dens}LAI, & if\ T_a > -1°C \\ (1.5T_a - 5.5)m_{scap}V_{dens}LAI, & if -3°C < T_a \leq -1°C \\ m_{scap}V_{dens}LAI & otherwise \end{cases} \tag{8}$$

620 where m_{scap} is a coefficient fixed to 5 (Andreadis et al., 2009). The dependency on air temperature S_{nv}^{max} allows the model to capture

the increase in snow loading resulting from increased adhesion and cohesion above $-3°C$ as recommended by Lundquist et al.

(2021). Snow unloading from trees follows the simple approach of Mazzotti et al. (2020a) with $U_{sv} = S_{nv}\frac{\Delta t}{\tau}$, with Δt the model

time step (s) and τ a relaxation time constant (s). This time constant is taken equal to 240 h for cold snow or 48 h for melting snow.

Finally, the sublimation of intercepted snow is estimated following Pomeroy et al. (1998) and Essery et al. (2003). In the version of

625 SVS2-Crocus used within this paper, unloaded snow is added to the snowfall and has the same physical properties (density and

microstructure) as falling snow (Mazzotti et al., 2024).

630

635

640

645

650 **Appendix B:** Profiles of density and SSA at TVC, Valley, Mixed Shrub and Shrub Tree
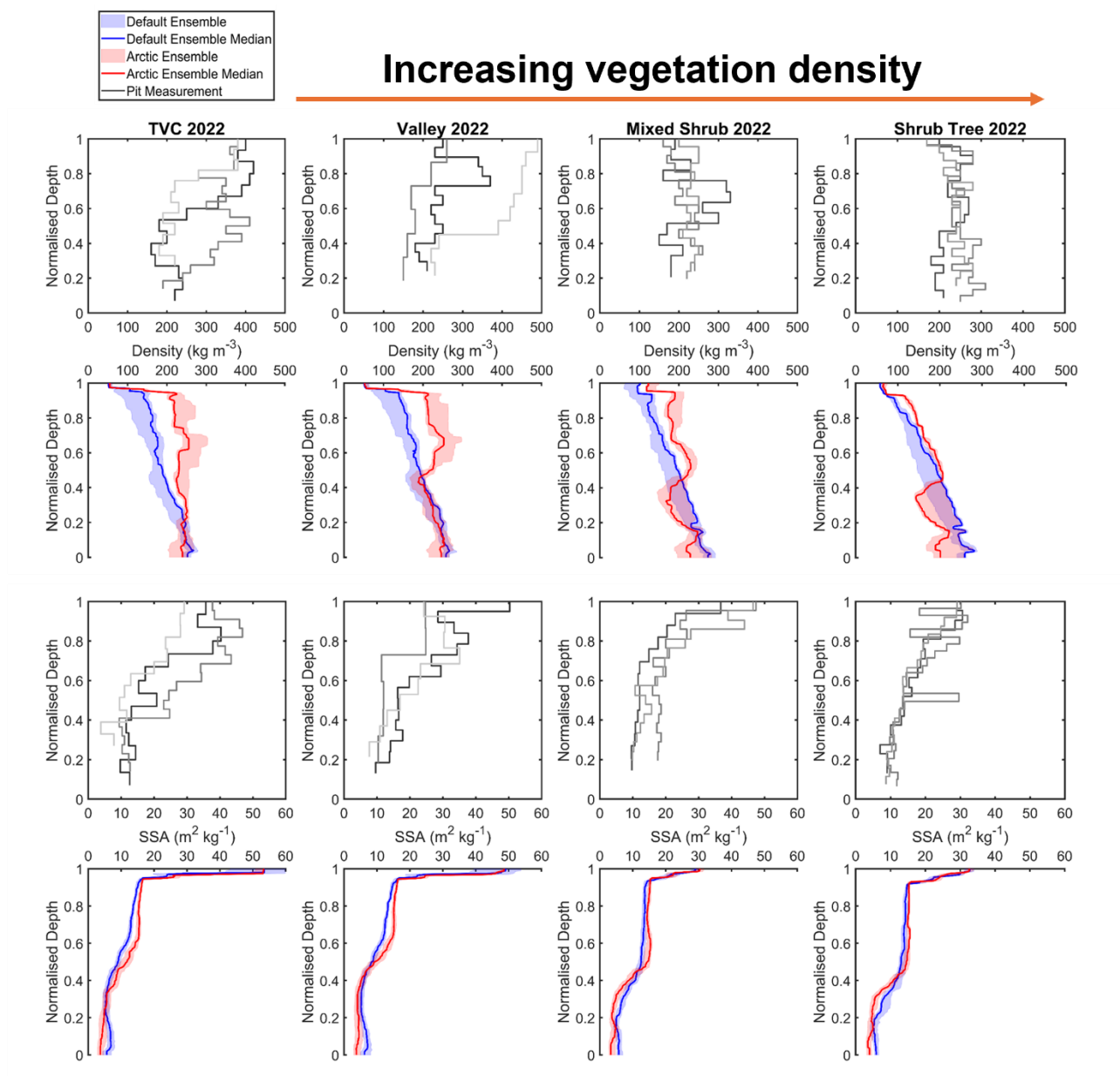
Figure B1. Comparison of measured and simulated vertical profiles of density (kg m^{-3}, median, interquartile range) and SSA (m^2 kg^{-1}, median, interquartile range) by default and Arctic SVS2-Crocus from the March 2022 winter field campaign. Black and grey lines indicate 655 different pit profiles. Vegetation type for each site is described in Fig. 1.
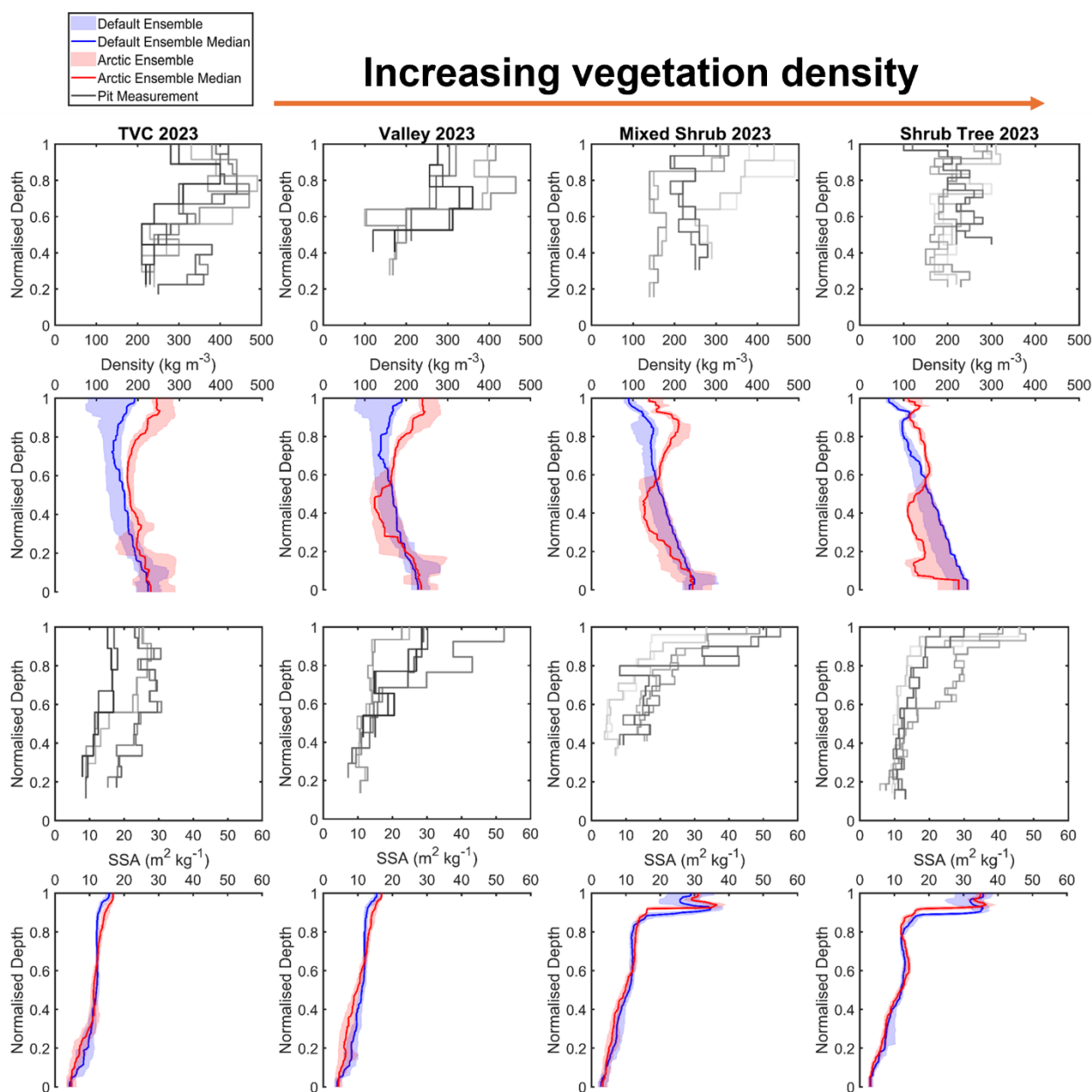
Figure B2. Comparison of measured and simulated vertical profiles of density (kg m^{-3}, median, interquartile range) and SSA (m^2 kg^{-1}, median, interquartile range) by default and Arctic SVS2-Crocus from the March 2023 winter field campaign. Black and grey lines indicate different pit profiles. Vegetation type for each site is described in Fig. 1.

Code and data availability. Code, simulated output and measurements to produce figures and meteorological forcing data are

665 available at: https://doi.org/10.5281/zenodo.15091024 (Woolley, 2025a). The version of Arctic SVS2-Crocus used within this study is available at: https://doi.org/10.5281/zenodo.15091095 (Woolley, 2025b)

Author Contributions: GJW conducted the simulations, analysis and drafted the manuscript. NR, LW, VV and CD supervised

670 the project. GJW, NR, VV, CD, RE, GHG and PM collected TVC snow measurements. GJW, VV and LW designed the SVS2-Crocus simulations. RE performed the analysis of the hemispherical photographs. NL and VV provided the HRPDS meteorological forcing data and developed the canopy module. GJW, JM and BM set up SMRT and designed the simulations. All authors participated in reviewing and editing the paper.

675 *Competing Interests:* Some authors are members of the editorial board of The Cryosphere.

Acknowledgements. GJW was supported by the Natural Environment Research Council (NERC)-funded ONE Planet Doctoral Training Partnership [NE/S007512/1], hosted jointly by Northumbria and Newcastle Universities. NR and LW were also supported by NERC [grant no. NE/W003686/1]. The project was conducted with approval issue with the Aurora Research

680 Institute, Aurora College (license nos. 16237, 16501 and 17232). The authors would like to acknowledge that this study occurred within the Inuvialuit Settlement Region located in western Canada.

685

690

695

7.0 References

Andreadis, K. M., Storck, P., and Lettenmaier, D. P.: Modeling snow accumulation and ablation processes in forested
700 environments, Water Resources Research, 45, 10.1029/2008wr007042, 2009.

Barrere, M., Domine, F., Decharme, B., Morin, S., Vionnet, V., and Lafaysse, M.: Evaluating the performance of coupled
snow–soil models in SURFEXv8 to simulate the permafrost thermal regime at a high Arctic site, Geoscientific Model
Development, 10, 3461-3479, 10.5194/gmd-10-3461-2017, 2017.

Bartlett, P. A., MacKay, M. D., and Verseghy, D. L.: Modified snow algorithms in the Canadian land surface scheme: Model
705 runs and sensitivity analysis at three boreal forest stands, Atmosphere-Ocean, 44, 207-222, 10.3137/ao.440301, 2006.

Belke-Brea, M., Domine, F., Boudreau, S., Picard, G., Barrere, M., Arnaud, L., and Paradis, M.: New Allometric Equations
for Arctic Shrubs and Their Application for Calculating the Albedo of Surfaces with Snow and Protruding Branches, Journal
of Hydrometeorology, 21, 2581-2594, 10.1175/jhm-d-20-0012.1, 2020.

Bonner, H. M., Raleigh, M. S., and Small, E. E.: Isolating forest process effects on modelled snowpack density and snow water
710 equivalent, Hydrological Processes, 36, 10.1002/hyp.14475, 2022.

Bouchard, B., Nadeau, D. F., and Domine, F.: Comparison of snowpack structure in gaps and under the canopy in a humid
boreal forest, Hydrological Processes, 36, 10.1002/hyp.14681, 2022.

Bouchard, B., Nadeau, D. F., Domine, F., Wever, N., Michel, A., Lehning, M., and Isabelle, P.-E.: Impact of intercepted and
sub-canopy snow microstructure on snowpack response to rain-on-snow events under a boreal canopy, The Cryosphere, 18,
715 2783-2807, 10.5194/tc-18-2783-2024, 2024.

Bouvet, L., Calonne, N., Flin, F., and Geindreau, C.: Heterogeneous grain growth and vertical mass transfer within a snow
layer under a temperature gradient, The Cryosphere, 17, 3553-3573, 10.5194/tc-17-3553-2023, 2023.

Brucker, L., Royer, A., Picard, G., Langlois, A., and Fily, M.: Hourly simulations of the microwave brightness temperature of
seasonal snow in Quebec, Canada, using a coupled snow evolution–emission model, Remote Sensing of Environment, 115,
720 1966-1977, 10.1016/j.rse.2011.03.019, 2011.

Brun, E., David, P., Sudul, M., and Brunot, G.: A numerical model to simulate snow-cover stratigraphy for operational
avalanche forecasting, Journal of Glaciology, 38, 1992.

Callaghan, T. V., Werkman, B. R., and Crawford, R. M. M.: The Tundra-Taiga Interface and Its Dynamics: Concepts and
Applications., Ambio, 6-14, 2002.

725 Callaghan, T. V., Johansson, M., Brown, R. D., Groisman, P. Y., Labba, N., Radionov, V., Bradley, R. S., Blangy, S., Bulygina,
O. N., Christensen, T. R., Colman, J. E., Essery, R. L. H., Forbes, B. C., Forchhammer, M. C., Golubev, V. N., Honrath, R.
E., Juday, G. P., Meshcherskaya, A. V., Phoenix, G. K., Pomeroy, J., Rautio, A., Robinson, D. A., Schmidt, N. M., Serreze,
M. C., Shevchenko, V. P., Shiklomanov, A. I., Shmakin, A. B., Sköld, P., Sturm, M., Woo, M.-k., and Wood, E. F.: Multiple
Effects of Changes in Arctic Snow Cover, Ambio, 40, 32-45, 10.1007/s13280-011-0213-x, 2012.

730 Carmagnola, C. M., Morin, S., Lafaysse, M., Domine, F., Lesaffre, B., Lejeune, Y., Picard, G., and Arnaud, L.: Implementation
and evaluation of prognostic representations of the optical diameter of snow in the SURFEX/ISBA-Crocus detailed snowpack
model, The Cryosphere, 8, 417-437, 10.5194/tc-8-417-2014, 2014.

Cui, Y., Xiong, C., Lemmetyinen, J., Shi, J., Jiang, L., Peng, B., Li, H., Zhao, T., Ji, D., and Hu, T.: Estimating Snow Water Equivalent with Backscattering at X and Ku Band Based on Absorption Loss, Remote Sensing, 8, 10.3390/rs8060505, 2016.

735 Derksen, C., Lemmetyinen, J., Toose, P., Silis, A., Pulliainen, J., and Sturm, M.: Physical properties of Arctic versus subarctic snow: Implications for high latitude passive microwave snow water equivalent retrievals, Journal of Geophysical Research: Atmospheres, 119, 7254-7270, 10.1002/2013jd021264, 2014.

Derksen, C., Silis, A., Sturm, M., Holmgren, J., Liston, G. E., Huntington, H., and Solie, D.: Northwest Territories and Nunavut Snow Characteristics from a Subarctic Traverse: Implications for Passive Microwave Remote Sensing, Journal of
740 Hydrometeorology, 10, 448-463, 10.1175/2008jhm1074.1, 2009.

Derksen, C., King, J., Belair, S., Garnaud, C., Vionnet, V., Fortin, V., Lemmetyinen, J., Crevier, Y., Plourde, P., Lawrence, B., van Mierlo, H., Burbidge, G., and Siqueira, P.: Development of the Terrestrial Snow Mass Mission, 2021 IEEE International Geoscience and Remote Sensing Symposium IGARSS, 10.1109/igarss47720.2021.9553496, 2021.

Domine, F., Barrere, M., and Morin, S.: The growth of shrubs on high Arctic tundra at Bylot Island: impact on snow physical
745 properties and permafrost thermal regime Biogeosciences Discussions, 10.5194/bg-2016-3, 2016.

Domine, F., Fourteau, K., Picard, G., Lackner, G., Sarrazin, D., and Poirier, M.: Permafrost cooled in winter by thermal bridging through snow-covered shrub branches, Nat Geosci, 15, 554-560, 10.1038/s41561-022-00979-2, 2022.

Domine, F., Picard, G., Morin, S., Barrere, M., Madore, J.-B., and Langlois, A.: Major Issues in Simulating Some Arctic Snowpack Properties Using Current Detailed Snow Physics Models: Consequences for the Thermal Regime and Water Budget
750 of Permafrost, Journal of Advances in Modeling Earth Systems, 11, 34-44, 10.1029/2018ms001445, 2019.

Ellis, C. R., Pomeroy, J. W., Brown, T., and MacDonald, J.: Simulation of snow accumulation and melt in needleleaf forest environments, Hydrology and Earth System Sciences, 14, 925-940, 10.5194/hess-14-925-2010, 2010.

Ernakovich, J. G., Hopping, K. A., Berdanier, A. B., Simpson, R. T., Kachergis, E. J., Steltzer, H., and Wallenstein, M. D.: Predicted responses of arctic and alpine ecosystems to altered seasonality under climate change, Glob Chang Biol, 20, 3256-
755 3269, 10.1111/gcb.12568, 2014.

Essery, R. and Pomeroy, J.: Vegetation and Topographic Control of Wind-Blown Snow Distributions in Distributed and Aggregated Simulations for an Arctic Tundra Basin, Journal of Hyrometeorology, 5, 735-744, https://doi.org/10.1175/1525-7541(2004)005<0735:VATCOW>2.0.CO;2, 2004.

Essery, R., Pomeroy, J., Ellis, C., and Link, T.: Modelling longwave radiation to snow beneath forest canopies using
760 hemispherical photography or linear regression, Hydrological Processes, 22, 2788-2800, 10.1002/hyp.6930, 2008.

Essery, R., Pomeroy, J., Parviainen, J., and Storck, P.: Sublimation of Snow from Coniferous Forests in a Climate Model, Journal of Climate, 16, 1855-1864, https://doi.org/10.1175/1520-0442(2003)016<1855:SOSFCF>2.0.CO;2, 2003.

Essery, R., Mazzotti, G., Barr, S., Jonas, T., Quaife, T., and Rutter, N.: A Flexible Snow Model (FSM 2.1.0) including a forest canopy, EGUsphere, 10.5194/egusphere-2024-2546, 2024.

765 Fierz, C., Armstrong, R. L., Durand, Y., Etchevers, P., Greene, E., McClung, D., Nishimura, K., Satyawali, P., and Sokratov, S. A.: The international classification for seasonal snow on the ground UNESCO, IHP-VII, Tech. Doc. Hydrol., 83, 2009.

Fortin, V., Abaza, M., Anctil, F., and Turcotte, R.: Why Should Ensemble Spread Match the RMSE of the Ensemble Mean?, Journal of Hydrometeorology, 15, 1708-1713, 10.1175/jhm-d-14-0008.1, 2014.

Fourteau, K., Domine, F., and Hagenmuller, P.: Impact of water vapor diffusion and latent heat on the effective thermal
770 conductivity of snow, The Cryosphere, 15, 2739-2755, 10.5194/tc-15-2739-2021, 2021.

Fung, A.: Microwave scattering and emission models and their applications, Boston: Artech House1994.

Gaillard, M., Vionnet, V., Lafaysse, M., Dumont, M., and Ginoux, P.: Improving large-scale snow albedo modeling using a
climatology of light-absorbing particle deposition, The Cryosphere, 19, 769-792, 10.5194/tc-19-769-2025, 2025.

Gallet, J.-C., Domine, F., Zender, C. S., and Picard, G.: Measurement of the specific surface area of snow using infrared
775 reflectance in an integrating sphere at 1310 and 1550 nm, The Cryosphere, 3, 167-182, 2009.

Garnaud, C., Bélair, S., Carrera, M. L., Derksen, C., Bilodeau, B., Abrahamowicz, M., Gauthier, N., and Vionnet, V.:
Quantifying Snow Mass Mission Concept Trade-Offs Using an Observing System Simulation Experiment, Journal of
Hydrometeorology, 20, 155-173, 10.1175/jhm-d-17-0241.1, 2019.

Gouttevin, I., Langer, M., Löwe, H., Boike, J., Proksch, M., and Schneebeli, M.: Observation and modelling of snow at a
780 polygonal tundra permafrost site: spatial variability and thermal implications, The Cryosphere, 12, 3693-3717, 10.5194/tc-12-
3693-2018, 2018.

Graveline, V., Helbig, M., Gosselin, G. H., Alcock, H., Detto, M., Walker, B., Marsh, P., and Sonnentag, O.: Surface-
atmosphere energy exchanges and their effects on surface climate and atmospheric boundary layer characteristics in the forest-
tundra ecotone in northwestern Canada, Agricultural and Forest Meteorology, 350, 10.1016/j.agrformet.2024.109996, 2024.

785 Hedstrom, N. R. and Pomeroy, J. W.: Measurements and modelling of snow interception in the boreal forest, Hydrological
Processes, 12, 1611-1625, 10.1002/(sici)1099-1085(199808/09)12:10/11<1611::Aid-hyp684>3.0.Co;2-4, 1998.

Kim, R. S., Kumar, S., Vuyovich, C., Houser, P., Lundquist, J., Mudryk, L., Durand, M., Barros, A., Kim, E. J., Forman, B.
A., Gutmann, E. D., Wrzesien, M. L., Garnaud, C., Sandells, M., Marshall, H.-P., Cristea, N., Pflug, J. M., Johnston, J., Cao,
Y., Mocko, D., and Wang, S.: Snow Ensemble Uncertainty Project (SEUP): quantification of snow water equivalent
790 uncertainty across North America via ensemble land surface modeling, The Cryosphere, 15, 771-791, 10.5194/tc-15-771-2021,
2021.

Kinar, N. J. and Pomeroy, J. W.: Measurement of the physical properties of the snowpack, Reviews of Geophysics, 53, 481-
544, 10.1002/2015rg000481, 2015.

King, J., Howell, S., Brady, M., Toose, P., Derksen, C., Haas, C., and Beckers, J.: Local-scale variability of snow density on
795 Arctic sea ice, The Cryosphere, 14, 4323-4339, 10.5194/tc-2019-305, 2020.

King, J., Kelly, R., Kasurak, A., Duguay, C., Gunn, G., Rutter, N., Watts, T., and Derksen, C.: Spatio-temporal influence of
tundra snow properties on Ku-band (17.2 GHz) backscatter, Journal of Glaciology, 61, 267-279, 10.3189/2015JoG14J020,
2015.

King, J., Derksen, C., Toose, P., Langlois, A., Larsen, C., Lemmetyinen, J., Marsh, P., Montpetit, B., Roy, A., Rutter, N., and
800 Sturm, M.: The influence of snow microstructure on dual-frequency radar measurements in a tundra environment, Remote
Sensing of Environment, 215, 242-254, 10.1016/j.rse.2018.05.028, 2018.

Krogh, S. A. and Pomeroy, J. W.: Impact of Future Climate and Vegetation on the Hydrology of an Arctic Headwater Basin
at the Tundra–Taiga Transition, Journal of Hydrometeorology, 20, 197-215, 10.1175/jhm-d-18-0187.1, 2019.

Lackner, G., Domine, F., Nadeau, D. F., Lafaysse, M., and Dumont, M.: Snow properties at the forest-tundra ecotone:
805 predominance of water vapour fluxes even in thick moderately cold snowpacks, The Cryosphere, 16, 3357-3373, 10.5194/tc-2022-19, 2022.

Lafaysse, M., Cluzet, B., Dumont, M., Lejeune, Y., Vionnet, V., and Morin, S.: A multiphysical ensemble system of numerical snow modelling, The Cryosphere, 11, 1173-1198, 10.5194/tc-11-1173-2017, 2017.

Larue, F., Royer, A., De Sève, D., Roy, A., Picard, G., Vionnet, V., and Cosme, E.: Simulation and Assimilation of Passive
810 Microwave Data Using a Snowpack Model Coupled to a Calibrated Radiative Transfer Model Over Northeastern Canada, Water Resources Research, 54, 4823-4848, 10.1029/2017wr022132, 2018.

Lemmetyinen, J., Kontu, A., Pulliainen, J., and Wiesmann, A.: Observations of seasonal snow cover at X and Ku bands during the NoSREx campaign, EUSAR 2014: 10th European Conference on Synthetic Aperture Radar, Berlin, Germany2014.

Lemmetyinen, J., Derksen, C., Rott, H., Macelloni, G., King, J., Schneebeli, M., Wiesmann, A., Leppänen, L., Kontu, A., and
815 Pulliainen, J.: Retrieval of Effective Correlation Length and Snow Water Equivalent from Radar and Passive Microwave Measurements, Remote Sensing, 10, 10.3390/rs10020170, 2018.

Libois, Q., Picard, G., Arnaud, L., Morin, S., and Brun, E.: Modeling the impact of snow drift on the decameter-scale variability of snow properties on the Antarctic Plateau, Journal of Geophysical Research: Atmospheres, 119, 11,662-611,681, 10.1002/2014jd022361, 2014.

820 Liston, G. E. and Elder, K.: A Meterological Distribution System for High-Resolution Terrestrial Modeling (MicroMet), Journal of Hydrometeorology, 7, 217-234, https://doi.org/10.1175/JHM486.1, 2006.

Lumbrazo, C., Bennett, A., Currier, W. R., Nijssen, B., and Lundquist, J.: Evaluating Multiple Canopy-Snow Unloading Parameterizations in SUMMA With Time-Lapse Photography Characterized by Citizen Scientists, Water Resources Research, 58, 10.1029/2021wr030852, 2022.

825 Lundquist, J. D., Dickerson-Lange, S., Gutmann, E., Jonas, T., Lumbrazo, C., and Reynolds, D.: Snow interception modelling: Isolated observations have led to many land surface models lacking appropriate temperature sensitivities, Hydrological Processes, 35, 10.1002/hyp.14274, 2021.

Marbouty, D.: An Experimental Study of Temperature-Gradient Metamorphism, Journal of Glaciology, 26, 303-312, 10.3189/s0022143000010844, 1980.

830 Marsh, P., Bartlett, P., MacKay, M., Pohl, S., and Lantz, T.: Snowmelt energetics at a shrub tundra site in the western Canadian Arctic, Hydrological Processes, 24, 3603-3620, 10.1002/hyp.7786, 2010.

Martin, J. and Schneebeli, M.: Impact of the sampling procedure on the specific surface area of snow measurements with the IceCube, The Cryosphere, 17, 1723-1734, 10.5194/tc-17-1723-2023, 2023.

Mazzotti, G., Essery, R., Moeser, C. D., and Jonas, T.: Resolving Small-Scale Forest Snow Patterns Using an Energy Balance
835 Snow Model With a One-Layer Canopy, Water Resources Research, 56, 10.1029/2019wr026129, 2020a.

Mazzotti, G., Essery, R., Webster, C., Malle, J., and Jonas, T.: Process-Level Evaluation of a Hyper-Resolution Forest Snow Model Using Distributed Multisensor Observations, Water Resources Research, 56, 10.1029/2020wr027572, 2020b.

Mazzotti, G., Nousu, J.-P., Vionnet, V., Jonas, T., Nheili, R., and Lafaysse, M.: Exploring the potential forest snow modelling at the tree and snowpack layer scale, EGUsphere, 10.5194/egusphere-2023-2781, 2024.

840 Mekonnen, Z. A., Riley, W. J., Berner, L. T., Bouskill, N. J., Torn, M. S., Iwahana, G., Breen, A. L., Myers-Smith, I. H., Criado, M. G., Liu, Y., Euskirchen, E. S., Goetz, S. J., Mack, M. C., and Grant, R. F.: Arctic tundra shrubification: a review of mechanisms and impacts on ecosystem carbon balance, Environmental Research Letters, 16, 10.1088/1748-9326/abf28b, 2021.

Meloche, J., Leroux, N. R., Montpetit, B., Vionnet, V., and Derksen, C.: Radar Equivalent Snowpack: reducing the number of
845 snow layers while retaining its microwave properties and bulk snow mass, EGUsphere, 10.5194/egusphere-2024-3169, 2024.

Ménard, C. B., Essery, R., Pomeroy, J., Marsh, P., and Clark, D. B.: A shrub bending model to calculate the albedo of shrub-tundra, Hydrological Processes, 28, 341-351, 10.1002/hyp.9582, 2014.

Milbrandt, J. A., Bélair, S., Faucher, M., Vallée, M., Carrera, M. L., and Glazer, A.: The pan-Canadian high resolution (2.5 km) deterministic prediction system., Weather and Forecasting., 31, 1791-1816, 2016.

850 Montesano, P. M., Neigh, C. S. R., Macander, M., Feng, M., and Noojipady, P.: The bioclimatic extent and pattern of the cold edge of the boreal forest: the circumpolar taiga-tundra ecotone, Environmental Research Letters, 15, 10.1088/1748-9326/abb2c7, 2020.

Montpetit, B., King, J., Meloche, J., Derksen, C., Siqueira, P., Adam, J. M., Toose, P., Brady, M., Wendleder, A., Vionnet, V., and Leroux, N. R.: Retrieval of snow and soil properties for forward radiative transfer modeling of airborne Ku-band SAR to
855 estimate snow water equivalent: the Trail Valley Creek 2018/19 snow experiment, The Cryosphere, 18, 3857-3874, 10.5194/tc-18-3857-2024, 2024.

Morin, S., Domine, F., Dufour, A., Lejeune, Y., Lesaffre, B., Willemet, J. M., Carmagnola, C. M., and Jacobi, H. W.: Measurements and modeling of the vertical profile of specific surface area of an alpine snowpack, Advances in Water Resources, 55, 111-120, 10.1016/j.advwatres.2012.01.010, 2013.

860 Mortimer, C., Mudryk, L., Derksen, C., Luojus, K., Brown, R., Kelly, R., and Tedesco, M.: Evaluation of long-term Northern Hemisphere snow water equivalent products, The Cryosphere, 14, 1579-1594, 10.5194/tc-14-1579-2020, 2020.

Musselman, K. N., Pomeroy, J. W., and Link, T. E.: Variability in shortwave irradiance caused by forest gaps: Measurements, modelling, and implications for snow energetics, Agricultural and Forest Meteorology, 207, 69-82, 10.1016/j.agrformet.2015.03.014, 2015.

865 Nill, L., Grünberg, I., Ullmann, T., Gessner, M., Boike, J., and Hostert, P.: Arctic shrub expansion revealed by Landsat-derived multitemporal vegetation cover fractions in the Western Canadian Arctic, Remote Sensing of Environment, 281, 10.1016/j.rse.2022.113228, 2022.

Oreiller, M., Nadeau, D. F., Minville, M., and Rousseau, A. N.: Modelling snow water equivalent and spring runoff in a boreal watershed, James Bay, Canada, Hydrological Processes, 28, 5991-6005, 10.1002/hyp.10091, 2014.

870 Pan, J., Durand, M. T., Vander Jagt, B. J., and Liu, D.: Application of a Markov Chain Monte Carlo algorithm for snow water equivalent retrieval from passive microwave measurements, Remote Sensing of Environment, 192, 150-165, 10.1016/j.rse.2017.02.006, 2017.

Picard, G., Sandells, M., and Löwe, H.: SMRT: an active–passive microwave radiative transfer model for snow with multiple microstructure and scattering formulations (v1.0), Geoscientific Model Development, 11, 2763-2788, 10.5194/gmd-11-2763-
875 2018, 2018.

Picard, G., Löwe, H., Domine, F., Arnaud, L., Larue, F., Favier, V., Le Meur, E., Lefebvre, E., Savarino, J., and Royer, A.: The Microwave Snow Grain Size: A New Concept to Predict Satellite Observations Over Snow-Covered Regions, AGU Advances, 3, 10.1029/2021av000630, 2022.

880   Pomeroy, J. W. and Dion, K.: Winter Radiation Extinction and Reflection in a Boreal Pine Canopy: Measurements and Modelling, Hydrological Processes, 10, 1591-1608, 10.1002/(sici)1099-1085(199612)10:12<1591::Aid-hyp503>3.0.Co;2-8, 1996.

Pomeroy, J. W., Parviainen, J., Hedstrom, N., and Gray, D. M.: Coupled modelling of forest snow interception and sublimation, Hydrological Processes, 12, 2317-2337, 10.1002/(sici)1099-1085(199812)12:15<2317::Aid-hyp799>3.0.Co;2-x, 1998.

Roth, T. R. and Nolin, A. W.: Forest impacts on snow accumulation and ablation across an elevation gradient in a temperate
885   montane environment, Hydrology and Earth System Sciences, 21, 5427-5442, 10.5194/hess-21-5427-2017, 2017.

Rott, H., Heidinger, M., Nagler, T., Cline, D., and Yueh, S.: Retrieval of Snow Parameters from Ku-Band and X-Band Radar Backscatter Measurements, IEEE International Geoscience and Remote Sensing Symposium 2009.

Royer, A., Domine, F., Roy, A., Langlois, A., Marchand, N., and Davesne, G.: New northern snowpack classification linked to vegetation cover on a latitudinal mega-transect across northeastern Canada, Écoscience, 28, 225-242,
890   10.1080/11956860.2021.1898775, 2021a.

Royer, A., Picard, G., Vargel, C., Langlois, A., Gouttevin, I., and Dumont, M.: Improved Simulation of Arctic Circumpolar Land Area Snow Properties and Soil Temperatures, Frontiers in Earth Science, 9, 2296-6463, 10.3389/feart.2021.685140, 2021b.

Rutter, N., Marshall, H. P., Tape, K., Essery, R., and King, J.: Impact of spatial averaging on radar reflectivity at internal
895   snowpack layer boundaries, Journal of Glaciology, 62, 1065-1074, 10.1017/jog.2016.99, 2016.

Rutter, N., Essery, R., Baxter, R., Hancock, S., Horton, M., Huntley, B., Reid, T., and Woodward, J.: Canopy Structure and Air Temperature Inversions Impact Simulation of Sub-Canopy Longwave Radiation in Snow-Covered Boreal Forests, Journal of Geophysical Research: Atmospheres, 128, 10.1029/2022jd037980, 2023.

Rutter, N., Sandells, M. J., Derksen, C., King, J., Toose, P., Wake, L., Watts, T., Essery, R., Roy, A., Royer, A., Marsh, P.,
900   Larsen, C., and Sturm, M.: Effect of snow microstructure variability on Ku-band radar snow water equivalent retrievals, The Cryosphere, 13, 3045-3059, 10.5194/tc-13-3045-2019, 2019.

Sandells, M., Rutter, N., Wivell, K., Essery, R., Fox, S., Harlow, C., Picard, G., Roy, A., Royer, A., and Toose, P.: Simulation of Arctic snow microwave emission in surface-sensitive atmosphere channels, The Cryosphere, 18, 3971-3990, 10.5194/tc-18-3971-2024, 2024.

905   Sokol, J., Pultz, T. J., and Walker, A. E.: Passive and active airborne microwave remote sensing of snow cover, International Journal of Remote Sensing, 24, 5327-2344, 10.1080/0143116031000115076, 2003.

Strasser, U., Warscher, M., Rottler, E., and Hanzer, F.: openAMUNDSEN v1.0: an open-source snow-hydrological model for mountain regions, Geoscientific Model Development, 17, 6775-6797, 10.5194/gmd-17-6775-2024, 2024.

Sturm, M. and Holmgren, J.: An Automatic Snow Depth Probe for Field Validation Campaigns, Water Resources Research,
910   54, 9695-9701, 10.1029/2018wr023559, 2018.

Sturm, M., Racine, C., and Tape, K.: Increasing shrub abundance in the Arctic, Nature, 411, 546-547, 2001.

Sturm, M., Holmgren, J., König, M., and Morris, K.: The thermal conductivity of seasonal snow, Journal of Glaciology, 43, 26-41, 10.3189/s0022143000002781, 1997.

Sun, N., Wigmosta, M., Zhou, T., Lundquist, J., Dickerson-Lange, S., and Cristea, N.: Evaluating the functionality and streamflow impacts of explicitly modelling forest–snow interactions and canopy gaps in a distributed hydrologic model, Hydrological Processes, 32, 2128-2140, 10.1002/hyp.13150, 2018.

Tsang, L., Durand, M., Derksen, C., Barros, A. P., Kang, D.-H., Lievens, H., Marshall, H.-P., Zhu, J., Johnson, J., King, J., Lemmetyinen, J., Sandells, M., Rutter, N., Siqueira, P., Nolin, A., Osmanoglu, B., Vuyovich, C., Kim, E., Taylor, D., Merkouriadi, I., Brucker, L., Navari, M., Dumont, M., Kelly, R., Kim, R. S., Liao, T.-H., Borah, F., and Xu, X.: Review article: Global monitoring of snow water equivalent using high-frequency radar remote sensing, The Cryosphere, 16, 3531-3573, 10.5194/tc-16-3531-2022, 2022.

Vionnet, V., Brun, E., Morin, S., Boone, A., Faroux, S., Le Moigne, P., Martin, E., and Willemet, J. M.: The detailed snowpack scheme Crocus and its implementation in SURFEX v7.2, Geoscientific Model Development, 5, 773-791, 10.5194/gmd-5-773-2012, 2012.

Vionnet, V., Verville, M., Fortin, V., Brugman, M., Abrahamowicz, M., Lemay, F., Thériault, J. M., Lafaysse, M., and Milbrandt, J. A.: Snow Level From Post-Processing of Atmospheric Model Improves Snowfall Estimate and Snowpack Prediction in Mountains, Water Resources Research, 58, 10.1029/2021wr031778, 2022.

Walker, B. and Marsh, P.: Snow depth, density, and snow water equivalent observations at Trail Valley Creek Research Station, Northwest Territories, 2015-2019 (V1), Borealis [dataset], doi/10.5683/SP2/RUSEHA, 2021.

Wang, X. and Baker, I.: Evolution of the specific surface area of snow during high-temperature gradient metamorphism, Journal of Geophysical Research: Atmospheres, 119, 10.1002/2014jd022131, 2014.

Weise, M.: Time-lapse tomography of mass fluxes and microstructural changes in snow, PhD thesis, ETH, Zurich, https://doi.org/10.3929/ethz-b-000213853, 2017.

Woolley, G. J.: Code and Data for Snow Properties and Ku-Band Backscatter (v1.0.0) [dataset], 10.5281/zenodo.15091024, 2025a.

Woolley, G. J.: Code for the Soil Vegetation and Snow version 2 (SVS2) land surface model (Woolley et al., 2025) (v1.0.0) [dataset], 10.5281/zenodo.15091095, 2025b.

Woolley, G. J., Rutter, N., Wake, L., Vionnet, V., Derksen, C., Essery, R., Marsh, P., Tutton, R., Walker, B., Lafaysse, M., and Pritchard, D.: Multi-physics ensemble modelling of Arctic tundra snowpack properties, The Cryosphere, 2024, 5685-5711, https://doi.org/10.5194/tc-18-5685-2024, 2024.

Zuanon, N.: IceCube, a portable and reliable instrument for snow specific surface area measurement in the field, International Snow Science Workshop Grenoble, Chamonix Mont-Blanc, 1020-1023,